JAMES
JOURNAL OF ADVANCES IN MODELING EARTH SYSTEMS

Idealized tropical cyclone simulations of intermediate complexity: A test case for AGCMs

Kevin A. Reed and Christiane Jablonowski

University of Michigan, Department of Atmospheric, Oceanic and Space Sciences, Ann Arbor, Michigan, USA

Manuscript submitted 30 November 2011

The paper introduces a moist, deterministic test case of intermediate complexity for Atmospheric General Circulation Models (AGCMs). We suggest pairing an AGCM dynamical core with simple physical parameterizations to test the evolution of a single, idealized, initially weak vortex into a tropical cyclone. The initial conditions are based on an initial vortex seed that is in gradient-wind and hydrostatic balance. The suggested "simple-physics" package consists of parameterizations of bulk aerodynamic surface fluxes for moisture, sensible heat and momentum, boundary layer diffusion, and large-scale condensation. Such a configuration includes the important driving mechanisms for tropical cyclones, and leads to a rapid intensification of the initial vortex over a forecast period of ten days. The simple-physics test paradigm is not limited to tropical cyclones, and can be universally applied to other flow fields. The physical parameterizations are described in detail to foster model intercomparisons.

The characteristics of the intermediate-complexity test case are demonstrated with the help of four hydrostatic dynamical cores that are part of the Community Atmosphere Model version 5 (CAM 5) developed at the National Center for Atmospheric Research (NCAR). In particular, these are the Finite-Volume, Spectral Element, and spectral transform Eulerian and semi-Lagrangian dynamical cores that are coupled to the simple-physics suite. The simulations show that despite the simplicity of the physics forcings the models develop the tropical cyclone at horizontal grid spacings of about 55 km and finer. The simple-physics simulations reveal essential differences in the storm's structure and strength due to the choice of the dynamical core. Similar differences are also seen in complex full-physics aqua-planet experiments with CAM 5 which serve as a motivator for this work. The results suggest that differences in complex full-physics simulations can be, at least partly, replicated in simplified model setups. The simplified experiments might therefore provide easier access to an improved physical understanding of how the dynamical core and moist physical parameterizations interact. It is concluded that the simple-physics test case has the potential to close the gap between dry dynamical core assessments and full-physics aqua-planet experiments, and can shed light on the role of the dynamical core in the presence of moisture processes.

1. Introduction

The testing of Atmospheric General Circulation Models (AGCMs) is an important component of continued model evaluation and improvement. Tests help reveal the impact of an individual AGCM's design on the model representation of the atmospheric circulation and climate. In the absence of simple analytic solutions, AGCMs are often evaluated by model intercomparisons like the Atmospheric Model Intercomparison Project (AMIP) (Gates, 1992; Gates et al., 1999). Such AMIP studies typically require AGCM simulations on the order of decades and are forced with prescribed, observation-based boundary data to investigate systematic errors of AGCMs. AMIP simulations are traditionally compared to global re-analysis data and observations, and to other AMIP runs from different AGCMs. However, identifying the reasons for model errors in these simulations still proves to be difficult due to the inherent complexity of AGCMs with full physical parameterization suites, complex boundary interactions, a land-sea mask and topography. Most often, the evaluation and interpretation of the results depend on the intuition and experience of the model development team.

Simpler model assessments can assist in identifying

To whom correspondence should be addressed.
Kevin A. Reed, Space Research Building, University of Michigan, 2455 Hayward St., Ann Arbor, MI, 48109, USA
e-mail: kareed@umich.edu

the causes and effects of the AGCM design choices more clearly. Here, we are particularly interested in the impact of the dynamical core on AGCM simulations while acknowledging that there are many other testbeds for physical parameterizations like the single column modeling approach (Betts and Miller, 1986; Randall et al., 1996). The dynamical core is the central fluid flow component of an AGCM. It not only determines the choice of the fluid flow equations, but also the numerical technique, computational grid, grid staggering options, and dissipation mechanisms. The latter are intended to mimic unresolved subgrid-scale processes and might also be paramount to keep the numerical scheme of the dynamical core stable (Jablonowski and Williamson, 2011). The impact of the modeling choices on the circulation in the presence of moisture and physical parameterizations is highly nonlinear and not well understood. The impact is especially difficult to evaluate in isolation in complex full-physics simulations which motivates a simpler setup.

Figure 1 displays the test hierarchy that is typically employed during the development phases of a dry dynamical core, and the coupled moist dynamics-physics AGCM at an advanced stage. The figure highlights the increases in complexity of the evaluation hierarchy from left to right. Typically, dynamical cores are first designed as 2D shallow water models on the sphere, which are the least complex models while capturing main aspects of the atmospheric flow, like large-scale Rossby waves. The design of 2D shallow water models necessitates choices for the horizontal and temporal numerical discretizations that inherently incorporate the grid and its staggering option, as well as the horizontal diffusion and filtering operations if required. Such 2D models are typically evaluated with the shallow water test suite by Williamson et al. (1992) or the barotropic instability test suggested by Galewsky et al. (2004). Shallow water tests are most often run for 5-15 simulation days, and thereby classify as deterministic test cases.

The second more complex class of dry dynamical core test cases depicted in Fig. 1 includes the vertical dimension. Either hydrostatic or non-hydrostatic, and shallow-atmosphere or deep-atmosphere designs are feasible (see White et al. (2005) for an overview of the equation sets). 3D test cases like the baroclinic instability test case by Jablonowski and Williamson (2006), Lauritzen et al. (2010) or Polvani et al. (2004), the 3D Rossby Haurwitz wave (Monaco and Williams, 1975; Giraldo and Rosmond, 2004) or the test suite by Jablonowski et al. (2008) are often used to assess the sensitivity of the dynamical core to the horizontal and vertical grid spacings, the impact of the computational grid, or the effects of the dissipation mechanisms. These aforementioned dynamical core tests are short deterministic test cases that can also assess the impact of idealized topography on the circulation. In addition, Held and Suarez (1994) and Boer and Denis (1997) suggested idealized evaluations of the model climate by introducing two simplified forcing mechanisms which serve as a "physical parameterization" package for the dynamical core. These forcing functions comprise a prescribed temperature relaxation and boundary layer friction that are applied during long-term ($\approx$1200-day) simulations on a flat and dry Earth. Typically, time-mean zonal-mean flow fields are analyzed to evaluate the mean climatic state and its variability, and differences amongst models can be, at least partly, traced back to differences in the dynamical cores. However, the spatial and temporal averaging of the model data smoothes out all small-scale features which makes it more difficult to isolate causes and effects in contrast to deterministic dynamical core evaluations.

The Held and Suarez (1994) climate assessments build bridges between the isolated dynamical core tests and full-physics experiments. But they neglect the highly nonlinear feedbacks between the dynamical core and physical parameterizations that are triggered by moisture processes. The latter are captured by aqua-planet experiments (APE, fourth box from the left in Fig. 1) as suggested by Neale and Hoskins (2000). APE studies are full-physics simulations that are forced with analytically prescribed sea surface temperatures (SSTs) on a flat and ocean-covered Earth. They thereby reduce the complexity of the boundary conditions while allowing the interaction of the dynamical core with the physical parameterizations. Typical APE studies are focused on the evaluation of the climatic state. They require long model integrations over several years as discussed by Williamson (2008a) or Mishra et al. (2011), and are generally compared to aqua-planet experiments of other AGCMs. In addition, short deterministic aqua-planet studies are feasible, as e.g. shown in the topical cyclone studies by Reed and Jablonowski (2011a,c,b).

The fifth and most complex category in Fig. 1 includes the AMIP studies mentioned earlier. They utilize spatially and temporally varying boundary conditions, as well as a realistic land-sea mask and topography. AMIP studies are typically conducted at a late stage of the dynamical core development cycle, before the atmospheric component is fully coupled to interactive ocean and ice

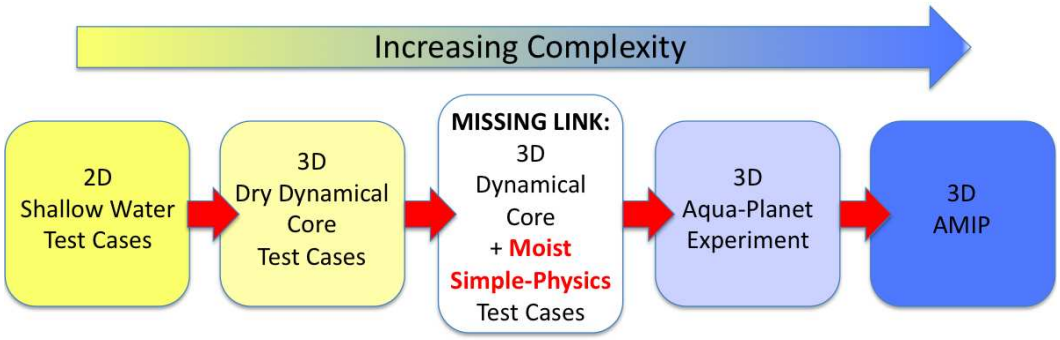

Figure 1: Diagram of the hierarchy of techniques for AGCM intercomparison and evaluation, emphasizing the need for intermediate complexity test cases.

models.

The jump in complexity between dry dynamical core test cases and APE and AMIP studies is quite substantial. The middle box of Fig. 1 accents the missing link between the dry and moist paradigms in the test hierarchy. We suggest that moist test cases of intermediate complexity can fill this void, and give an easier access to an improved understanding of the dynamics-physics interplay. This is especially true, if the new test case can mimic at least some of the behavior of complex full-physics simulations. The purpose of this paper is to suggest such a test case of intermediate complexity, and to demonstrate its characteristics with the help of an idealized tropical cyclone (Reed and Jablonowski, 2011a). Our study is motivated by the observation that the representation of the idealized tropical cyclones in full-physics aqua-planet studies is highly sensitive to the choice of the AGCM dynamical core. This raises the question whether the key dynamics-physics interactions can already be captured by simplified physical forcing mechanisms and whether the outcomes resemble, to some degree, the full-physics studies. The characteristics of the test case are shown for four hydrostatic dynamical cores that are part of the Community Atmosphere Model CAM version 5 (CAM 5, Neale et al. (2010b)) developed at the National Center for Atmospheric Research (NCAR). These are the current CAM 5 default Finite-Volume (FV) model, the Spectral Element (SE) model that is sometimes also called the Higher Order Method Modeling Environment (HOMME), as well as the Eulerian (EUL) and semi-Lagrangian (SLD) spectral transform dynamical cores.

Specifically, we propose pairing the AGCM dynamical cores with simple moist physical parameterizations to test the evolution of a single, idealized, initially weak vortex into a tropical cyclone over ten simulation days. This test requires the definition of the initial conditions, as explained in detail in Reed and Jablonowski (2011a), and the definition of the reduced moist parameterization suite (called "simple-physics" hereafter), described in this paper. The initial conditions are analytic, allowing for an easy implementation on any computational grid. The simple-physics suite contains all necessary drivers for tropical cyclones, including large-scale condensation, surface fluxes and boundary layer turbulence. We note that the implementation of reduced physics packages within AGCMs has been introduced before (e.g. by Molteni (2002) and Frierson et al. (2006)), and the resulting models are sometimes characterized as Earth System Models of Intermediate Complexity (EMICs). The latter also include simplified ocean, ice and land models that are most often run at low resolutions over many decades (Claussen et al., 2002). However, there are two main differences to such earlier studies. First, we provide the complete description of the simple-physics package, its implementation and the physics-dynamics coupling strategy, which is paramount for model intercomparisons. Second, the simple-physics package described here is even more simplified than other comparable approaches, e.g. we leave out a radiative transfer scheme which can be justified for short deterministic model runs. The tropical cyclone serves as an example scenario. However, the simple-physics test paradigm is universal and and can also be applied to other flow fields.

The paper is organized as follows. The simple-physics suite is introduced in detail in section 2. Section 3 briefly reviews the design of NCAR's four CAM 5 dynamical cores and their horizontal grid spacings.

The APE simulation results for each dynamical core with the full CAM 5 physics suite are presented in section 4. These full-physics simulations serve as a motivation for the more simplified physics assessments. The simple-physics experiments with each of the CAM 5 dynamical cores are then presented in section 5, along with an assessment of the model uncertainty. Section 6 summarizes our conclusions and outlines potential future research. A brief description of the initial conditions, the hybrid vertical coordinate of the model CAM 5, and the details about the implementation of the simple-physics suite are provided in the appendices.

2. Introduction of the simple-physics parameterization suite

This section introduces the components of the simplified physical parameterization package called simple-physics. It contains selected physical processes that are important driving mechanisms for tropical cyclones such as

1. large-scale condensation defined to occur when the atmosphere becomes saturated.

2. surface fluxes of horizontal momentum, evaporation (specific humidity) and sensible heat (temperature) from the ocean surface to the lower atmosphere.

3. boundary layer turbulence of horizontal momentum, temperature and specific humidity.

Each component is explained in detail below to foster model intercomparisons. The simple-physics package assumes an ocean-covered (aqua-planet) Earth with a uniform SST of 29 °C. This temperature matches the SST of the initial conditions that trigger a spin-up of a tropical cyclone as described in Reed and Jablonowski (2011a) and Appendix A. However, the simple-physics package is not limited to the tropical cyclone study used here for demonstration purposes. It can also be employed to explore other flow phenomena such as rainfall patterns in the presence of idealized mountains in the midlatitudes. The latter can be built upon test case 5-0-0 described in Jablonowski et al. (2008) with an adjusted SST which matches the initial surface temperature of this test case.

2.1. Large-scale condensation

The first component of the simple-physics package is the parameterization of large-scale condensation, and follows the approach used by many AGCMs, like the Integrated Forecasting System (IFS) of the European Centre for Medium-Range Weather Forecasts (Tiedtke, 1987). The large-scale condensation scheme does not include a cloud stage. No condensate is carried and the excess moisture is removed instantaneously without re-evaporation at lower levels. The model equations for the time rate of change of temperature T and specific humidity q due to condensation are

$$\frac{\partial T}{\partial t} = \frac{L}{c_p} C \tag{2.1}$$

$$\frac{\partial q}{\partial t} = -C, \tag{2.2}$$

where L is the latent heat of vaporization at 0 °C ($= 2.5 \times 10^6$ J kg^{-1}) and c_p is the specific heat of dry air ($= 1004.64$ J kg^{-1} K^{-1}). The condensation rate C is the rate at which the saturation specific humidity q_{sat} changes with time t

$$C = \frac{\mathrm{d}q_{sat}}{\mathrm{d}t}. \tag{2.3}$$

If the air is found to be supersaturated (that is $q > q_{sat}(T,p)$, where p is pressure) T and q need to be adjusted to their saturation values, which will lead to the updated values T^{n+1} and q^{n+1} at the future time level $n+1$

$$T^{n+1} = T + \triangle T \tag{2.4}$$

$$q^{n+1} = q + \triangle q. \tag{2.5}$$

The time index of the T and q values on the right hand side (RHS) of these equations depends upon the AGCM design which might enforce constraints on the suitable physics-dynamics coupling strategy. Two coupling strategies are common which are called process-split and time-split (Williamson, 2002). In models with process-split physics-dynamics coupling T and q represent either the values at the current time level (n) for two-time-level schemes or the values at the previous time level ($n-1$) for three-time-level schemes, like e.g. the leapfrog method used in CAM 5 EUL (Neale et al., 2010b). In time-split models, the values of T and q are already partially updated by the time tendencies of the dynamical core before physical forcings are invoked. We

leave the specific choice of the physics-dynamics coupling to the modeling group. However, in case no prior constraints exist we recommend the time-split approach. Note, pressure p is assumed to be time-invariant during individual physics parameterizations. This is a common assumption in AGCMs since the moist pressure is typically adjusted exactly once at the very end of the physics suite as further outlined in section 2.4.

The correction factors $\triangle T$ and $\triangle q$ are given by

$$\triangle T = -\frac{L}{c_p}\triangle q \quad (2.6)$$

$$\triangle q = q_{sat}(T^{n+1}, p) - q. \quad (2.7)$$

Here $q_{sat}(T^{n+1}, p)$ is approximated by a first-order Taylor series

$$q_{sat}(T^{n+1}, p) \cong q_{sat}(T, p) + \frac{\mathrm{d}q_{sat}(T, p)}{\mathrm{d}T}\triangle T. \quad (2.8)$$

The derivative of $q_{sat}(T, p)$ with respect to T appears as a full derivative since p remains unchanged during the physics time step. The forms of T^{n+1} and q^{n+1} are then represented by

$$T^{n+1} = T + \frac{L}{c_p}\frac{q - q_{sat}(T, p)}{1 + \frac{L}{c_p}\frac{\mathrm{d}q_{sat}(T,p)}{\mathrm{d}T}} \quad (2.9)$$

$$q^{n+1} = q - \frac{q - q_{sat}(T, p)}{1 + \frac{L}{c_p}\frac{\mathrm{d}q_{sat}(T,p)}{\mathrm{d}T}}. \quad (2.10)$$

This leads to the expression of the condensation rate for models with two-time-level schemes

$$C = \frac{1}{\triangle t}\left(\frac{q - q_{sat}(T, p)}{1 + \frac{L}{c_p}\frac{\mathrm{d}q_{sat}(T,p)}{\mathrm{d}T}}\right) \quad (2.11)$$

where $\triangle t$ symbolizes the discrete physics time step. Note that the physics time step may be different from the dynamics or tracer advection time steps as it is the case in the model CAM 5 FV (Neale et al., 2010b). In models with a three-time-level leapfrog scheme, $\triangle t$ needs to be replaced with $2\triangle t$.

We now need to define the derivative of the saturated specific humidity with respect to temperature. From Holton (2004) we approximate this to be

$$\frac{\mathrm{d}q_{sat}(T, p)}{\mathrm{d}T} \approx \frac{\varepsilon}{p}\frac{\mathrm{d}e_s(T)}{\mathrm{d}T} = \frac{Lq_{sat}(T, p)}{R_\nu T^2} \quad (2.12)$$

where e_s is the saturation vapor pressure, R_ν is the gas constant for water vapor ($= 461.5$ J kg^{-1} K^{-1}) and ε is the ratio of the gas constant for dry air R_d ($= 287.04$ J kg^{-1} K^{-1}) to that for water vapor ($\varepsilon = 0.622$). We approximate the saturation specific humidity by utilizing the Clausius-Clapeyron equation for the saturation vapor pressure in the form

$$q_{sat}(T, p) \approx \varepsilon\frac{e_s(T)}{p} \approx \frac{\varepsilon}{p}e_0^* e^{-(L/R_\nu)[(1/T)-(1/T_0)]} \quad (2.13)$$

where e_0^* ($= 610.78$ Pa) is the saturation vapor pressure at $T_0 = 273.16$ K. This formulation was also used in Frierson et al. (2006) for idealized model simulations. As mentioned before, it is assumed that all of the condensed water vapor immediately falls out as precipitation without re-evaporation. The large-scale precipitation rate P_{ls} is therefore given as

$$P_{ls} = \frac{1}{\rho_{water}}\int_0^\infty C\rho\mathrm{d}z = \frac{1}{\rho_{water}g}\int_0^{p_s} C\mathrm{d}p \quad (2.14)$$

where the hydrostatic relation is used to eliminate the air density ρ, $\rho_{water} = 1000$ kg m^{-3} is the density of water, g = 9.80616 m s^{-2} is the gravity and p_s is the surface pressure. The units of P_{ls} are meters of water per second (m$_{H_2O}$ s^{-1}). The quantity P_{ls} can be used as a diagnostic quantity.

2.2. Surface fluxes

The second component of the simple-physics package is the parameterization of the interaction of the atmosphere with the ocean surface. These fluxes also determine the eddy diffusivities for the boundary layer parameterization as explained in section 2.3. To parameterize the surface fluxes that impact the zonal velocity u, the meridional velocity v, temperature and moisture we start with the time rate of change equations

$$\frac{\partial u}{\partial t} = -\frac{1}{\rho}\frac{\partial\rho\,\overline{w'u'}}{\partial z} \quad (2.15)$$

$$\frac{\partial v}{\partial t} = -\frac{1}{\rho}\frac{\partial\rho\,\overline{w'v'}}{\partial z} \quad (2.16)$$

$$\frac{\partial T}{\partial t} = -\frac{1}{\rho}\frac{\partial\rho\,\overline{w'T'}}{\partial z} \quad (2.17)$$

$$\frac{\partial q}{\partial t} = -\frac{1}{\rho}\frac{\partial\rho\,\overline{w'q'}}{\partial z}. \quad (2.18)$$

Here u', v', w', T' and q' symbolize the deviations of the zonal velocity, meridional velocity, vertical velocity, temperature and specific humidity from their time averages, repectively. A time average is indicated by an overbar. For non-hydrostatic models the time rate of change

equations for the vertical velocity $\frac{\partial w}{\partial t}$ should be set to zero.

The eddy turbulence surface momentum fluxes on the RHS of Eqs. (2.15) and (2.16) are approximated by the bulk aerodynamic formulae in kinematic units

$$(\overline{w'u'})_s = -C_d|\vec{v}_a|u_a \quad (2.19)$$
$$(\overline{w'v'})_s = -C_d|\vec{v}_a|v_a, \quad (2.20)$$

where the subscript s denotes a surface flux. $|\vec{v}_a|$ is the wind speed of the horizontal wind ($|\vec{v}_a| = \sqrt{u_a^2 + v_a^2}$) at the lowermost model level, and u_a and v_a are the zonal and meridional wind components, respectively. This formulation of the surface fluxes implies that the wind velocities at the height of the ocean surface $z_0 = 0$ m are zero ($u_s = v_s = 0$ m s^{-1}), thereby forcing the stress to vanish at z_0. Here the drag coefficient, C_d, depends on the magnitude of the wind at the lowermost model level

$$\begin{array}{ll} C_d = C_{d0} + C_{d1}|\vec{v}_a| & \text{for } |\vec{v}_a| < 20 \text{ m s}^{-1} \\ C_d = 0.002 & \text{for } |\vec{v}_a| \geq 20 \text{ m s}^{-1}, \end{array} \quad (2.21)$$

where C_{d0} and C_{d1} are defined in Smith and Vogl (2008) to be 7.0×10^{-4} and 6.5×10^{-5} s m^{-1}, respectively, as derived from Black et al. (2007).

Evaporation occurs at the surface and is similarly described by the kinematic eddy flux of water vapor. It is expressed via the bulk formula for latent heat

$$(\overline{w'q'})_s = C_E|\vec{v}_a|(q_{sat,s} - q_a), \quad (2.22)$$

where q_a is the specific humidty of the lowermost model level and C_E is the bulk transfer coefficient for water vapor. $q_{sat,s}$ is the saturation specific humidity (Eq. (2.13)) computed with the SST value, which is 302.15 K for the tropical cyclone test case, and the surface pressure (Hasse and Smith, 1997). The kinematic eddy sensible heat flux at the surface is defined by the bulk formula

$$(\overline{w'T'})_s = C_H|\vec{v}_a|(T_s - T_a), \quad (2.23)$$

where C_H is the bulk heat transfer coefficient, T_a is the temperature of the lowermost model level and T_s is the surface temperature, with T_s taken to be the SST. For both evaporation and sensible heat the bulk coefficient is set to a constant, $C_E = C_H = 0.0011$, as suggested by Garratt (1992), Hasse and Smith (1997), and Smith and Vogl (2008) for ocean surfaces. All fluxes are specified in kinematic units which are m^2 s^{-2} for the momentum fluxes, K m s^{-1} for the sensible heat flux and (kg$_{vapor}$ kg$_{air}^{-1}$) (m s^{-1}) for the evaporation flux. If required, energy-based physical units (W m^{-2}) can be recovered if the horizontal momentum fluxes (Eqs. (2.19) and (2.20)) are multiplied by the density at the lowermost model level ρ_a, the latent heat flux (Eq. (2.22)) is multiplied by $\rho_a c_p$, and the sensible heat flux (Eq. (2.23)) is multiplied by $\rho_a L$. However, the implementation presented here utilizes kinematic fluxes. A positive flux denotes an upward transfer from the ocean surface into the atmosphere.

The surface fluxes (Eqs. (2.15) - (2.18)) are used to calculate the respective time tendencies of the state variables u, v, q and T at the lowermost model level. The spatially discretized form yields

$$\frac{\partial u_a}{\partial t} = -\frac{1}{\rho_a}\frac{\rho_a\,(\overline{w'u'})_a - \rho_s\,(\overline{w'u'})_s}{z_a - z_0} \quad (2.24)$$
$$\frac{\partial v_a}{\partial t} = -\frac{1}{\rho_a}\frac{\rho_a\,(\overline{w'v'})_a - \rho_s\,(\overline{w'v'})_s}{z_a - z_0} \quad (2.25)$$
$$\frac{\partial T_a}{\partial t} = -\frac{1}{\rho_a}\frac{\rho_a\,(\overline{w'T'})_a - \rho_s\,(\overline{w'T'})_s}{z_a - z_0} \quad (2.26)$$
$$\frac{\partial q_a}{\partial t} = -\frac{1}{\rho_a}\frac{\rho_a\,(\overline{w'q'})_a - \rho_s\,(\overline{w'q'})_s}{z_a - z_0}. \quad (2.27)$$

Again, the subscripts s and a represent the quantities at the surface and lowermost model level, repectively. z_a is defined as the height (in m) of the lowermost full model level and can be expressed with the help of the hydrostatic equation in terms of pressure

$$z_a = \frac{R_d T_{\nu,a}}{g}\frac{(\ln p_- - \ln p_s)}{2}, \quad (2.28)$$

where $T_{\nu,a} = T_a(1 + 0.608 q_a)$ is the virtual temperature at the lowermost full model level and p_- is the edge pressure at the model level interface between the lowest and second lowest full model levels. This notation and all previous and following equations assume that the temperature, horizontal wind components and the specific humidity in the physical parameterization package are co-located in both the vertical and horizontal directions, as it is the case for the Lorenz grid (Lorenz, 1960) and Arakawa-A grid (Arakawa and Lamb, 1977). Most often, AGCMs utilize such a co-located, possibly interpolated, grid in the physical parameterization suite, regardless of the staggering option in the dynamical core. If other vertical or horizontal grid staggering options are utilized in the physics package, the exact forms of the surface flux and boundary layer equations need to be adjusted accordingly.

All eddy fluxes at the lowermost model level (e.g. $(\overline{w'u'})_a$) are now set to zero, as all turbulent contributions from above the lowermost model level are accounted for in the boundary layer scheme described later

in section 2.3. This results in the following form of the surface fluxes and illustrates how they impact the time tendencies at the lowest model level

$$\frac{\partial u_a}{\partial t} = -\frac{1}{\rho_a}\frac{-\rho_s\,(\overline{w'u'})_s}{z_a} \quad (2.29)$$

$$\frac{\partial v_a}{\partial t} = -\frac{1}{\rho_a}\frac{-\rho_s\,(\overline{w'v'})_s}{z_a} \quad (2.30)$$

$$\frac{\partial T_a}{\partial t} = -\frac{1}{\rho_a}\frac{-\rho_s\,(\overline{w'T'})_s}{z_a} \quad (2.31)$$

$$\frac{\partial q_a}{\partial t} = -\frac{1}{\rho_a}\frac{-\rho_s\,(\overline{w'q'})_s}{z_a}. \quad (2.32)$$

ρ_s is the density at the surface, which for simplicity is assumed to be equal to ρ_a due to the typically chosen proximity of the lowermost model level to the surface. Therefore, we let the terms cancel. In our CAM 5 tropical cyclone tests presented later in sections 4 and 5 with a hybrid σ-pressure vertical coordinate (see Appendix B and Simmons and Burridge (1981)), the height position of the lowermost full model level is about $z_a = 70$ m. We define this height as the approximate height of the surface layer. Since the strength of the surface forcing is impacted by this choice, we encourage the users of this test case to pick about the same height position for their lowermost full model level. In any case, the approximate position of z_a needs to be documented.

The final form of the surface fluxes is

$$\frac{\partial u_a}{\partial t} = -\frac{C_d|\vec{v}_a|u_a}{z_a} \quad (2.33)$$

$$\frac{\partial v_a}{\partial t} = -\frac{C_d|\vec{v}_a|v_a}{z_a} \quad (2.34)$$

$$\frac{\partial T_a}{\partial t} = \frac{C_H|\vec{v}_a|(T_s - T_a)}{z_a} \quad (2.35)$$

$$\frac{\partial q_a}{\partial t} = \frac{C_E|\vec{v}_a|(q_{sat,s} - q_a)}{z_a}. \quad (2.36)$$

We again note that the wind at the surface is taken to be zero and therefore does not appear explicitly in Eqs. (2.33) and (2.34). All time derivatives of the surface fluxes are discretized in a semi-implicit way to avoid numerical instabilities, which is detailed in Appendix C.

The final form of the surface fluxes will vary for models with other choices of prognostic variables. For example, if potential temperature Θ_a is used Eq. (2.35) takes the form

$$\frac{\partial \Theta_a}{\partial t} = \frac{C_H|\vec{v}_a|(T_s - T_a)}{z_a}\left(\frac{p_{00}}{p_a}\right)^{R_d/c_p} \quad (2.37)$$

where $p_{00} = 10^5$ Pa is a reference pressure. This conversion uses the assumption that the pressure is time-invariant when individual physics parameterizations are applied. For other choices of prognostic variables like $(\rho u)_a$, $(\rho v)_a$, $(\rho\Theta)_a$ and $(\rho q)_a$ the right-hand-side of Eqs. (2.33), (2.34), (2.37) and (2.36) would need to be multiplied by ρ_a.

2.3. Boundary layer diffusion

The final component of the simple-physics package is the parametrization of a simple diffusive boundary layer. Potential temperature, as opposed to temperature, is used in the boundary layer parameterization because the vertical profile of the potential temperature is a suitable indicator of static stability. The base equation set for the boundary layer diffusion is described by Eqs. (2.15)-(2.18). However, the time rate of change equation of potential temperature Θ replaces the temperature tendency in Eq. (2.17). It yields

$$\frac{\partial \Theta}{\partial t} = -\frac{1}{\rho}\frac{\partial \rho\,\overline{w'\Theta'}}{\partial z}. \quad (2.38)$$

The potential temperature tendency can be converted back to a temperature T tendency of the following form

$$\frac{\partial T}{\partial t} = -\frac{1}{\rho}\left(\frac{p}{p_{00}}\right)^{R_d/c_p}\frac{\partial \rho\,\overline{w'\Theta'}}{\partial z}. \quad (2.39)$$

Again, this conversion assumes that the pressure is time-invariant during the application of the diffusion. The partial derivatives with respect to height in this and all following equations can also be converted to pressure-based derivatives using the hydrostatic approximation. This is explained in detail in Appendix D.

Boundary layers in rotating flows have special characteristics, as seen with Ekman theory. First-order approximations to the representation of boundary layers within hurricanes have been found to resemble Ekman-like profiles, where turbulent mixing is characterized by a constant vertical eddy diffusivity K_m (see Bode and Smith (1975)). Such turbulent mixing is characterized as

$$\overline{w'u'} = -K_m\frac{\partial u}{\partial z} \quad (2.40)$$

$$\overline{w'v'} = -K_m\frac{\partial v}{\partial z} \quad (2.41)$$

$$\overline{w'\Theta'} = -K_E\frac{\partial \Theta}{\partial z} \quad (2.42)$$

$$\overline{w'q'} = -K_E\frac{\partial q}{\partial z}, \quad (2.43)$$

where K_m is the eddy diffusivity coefficient for momentum and K_E is the eddy diffusivity coefficient for energy, which is most often set equal to that for water vapor.

Similar to Bode and Smith (1975) we match the eddy diffusivity to the wind stress sublayer which we calculated earlier to be the surface momentum flux at the lowermost model level. Therefore to first-order, we approximate K_m from the following formulation of the vertical turbulent flux of zonal momentum $\overline{w'u'}$ and demand that it matches $(\overline{w'u'})_s$ at the lowermost layer

$$(\overline{w'u'})_s = -K_m \frac{\partial u}{\partial z}. \tag{2.44}$$

At the lowermost model level this corresponds to the expression

$$-C_d|\vec{v}_a|u_a = -K_m \frac{u_a}{\triangle z} \tag{2.45}$$

in the discretized form, where $\triangle z$ is the height difference between z_a and z_0, and therefore $\triangle z = z_a$ (e.g. see Eq. (2.28)). As before, we recommend selecting the lowermost full model level at a height of about 70 m to allow for intercomparisons to the results presented later. One last time we utilize the lower boundary condition that the wind velocities at the height of the ocean surface z_0 are zero. For simplicity the boundary layer is defined to be all levels with pressure values greater than $p_{top} =$ 850 hPa (corresponding to a boundary layer height of approximately 1-1.5 km). Solving Eq. (2.45) for K_m and tapering the eddy diffusivity to zero above p_{top} gives

$$\begin{aligned} K_m &= C_d|\vec{v}_a|z_a && \text{for } p > p_{top} \\ K_m &= C_d|\vec{v}_a|z_a \exp\left(-\left[\tfrac{p_{top}-p}{p_{strato}}\right]^2\right) && \text{for } p \leq p_{top}. \end{aligned} \tag{2.46}$$

where we let K_m go to zero to ensure a smooth transition above the boundary layer. Here the constant p_{strato} determines the rate of decrease and is set to 100 hPa. This choice of p_{strato} lets K_m decrease by a factor of ten at the 700 hPa level. Similarly, K_E is defined by

$$\begin{aligned} K_E &= C_E|\vec{v}_a|z_a && \text{for } p > p_{top} \\ K_E &= C_E|\vec{v}_a|z_a \exp\left(-\left[\tfrac{p_{top}-p}{p_{strato}}\right]^2\right) && \text{for } p \leq p_{top}. \end{aligned} \tag{2.47}$$

These eddy diffusivities, and therefore the turbulent mixing, varies in space and time depending upon the magnitude of the horizontal wind $|\vec{v}_a|$ and the height z_a of the lowermost model level. This method reflects a simplified first-order coupling of the boundary layer diffusion to the dynamic conditions while omitting more complicated mechanisms such as the dependence of the eddy diffusivities on static stability indicators like Richardon numbers. This simplification of the boundary layer diffusivities is a deliberate choice. The boundary layer scheme is implemented with a partially implicit temporal discretization to avoid numerical instabillties. The details are explained in Appendix D.

2.4. Coupling of the simple-physics processes

The simple-physics suite is invoked with the state variables u, v, q, T from the dynamical core. These might already be partially updated (time-split) or might not be updated (process-split) with the time tendencies from the dynamical core. This physics-dynamics coupling choice depends upon possible constraints imposed by the dynamical core as outlined in section 2.1 or Williamson (2002). However, within the simple-physics parameterization suite all processes are coupled via time-splitting. With time-split coupling the individual physical parameterizations are applied sequentially and each component is based on the updated state provided by the previous process. The components are time-split in the following order:

1. The large-scale condensation scheme loops over all vertical levels at each horizontal grid point. It readily updates T and q throughout the vertical column using Eqs. (2.9)-(2.10).

2. Next, the updated T, q state variables and u, v wind components are used in the implementation of the surface fluxes. These variables are updated at the lowermost full model level according to Eqs. (C.3)-(C.6).

3. All state variables throughout the column are then updated with the boundary layer scheme and supplied back to the dynamical core for the calculations of the next time step. The boundary layer updates are described by Eqs. (D.15), (D.21), (D.28) and (D.31).

At the end of the simple-physics suite care needs to be taken to ensure that the model conserves the total dry air mass or its analog, the global average of the dry surface pressure. This is especially true if the moist surface pressure is predicted in the dynamical core, as it is the case in CAM 5. The adjustment can take place in either the dynamical core or at the end of the physics package

which again depends on the AGCM design. Most often, AGCMs already provide a mechanism to ensure that the total dry air mass is conserved, such as global mass fixers or explicit dry air adjustment routines as discussed in e.g. Neale et al. (2010b). If not, such a mechanism needs to be supplied. If the total amount of dry air needs to be prescribed, the initial conditions as provided in Reed and Jablonowski (2011a) contain a globally averaged dry surface pressure of about 1010 hPa.

2.5. Additional design choices

As mentioned before, we recommend placing the lowermost full model level at a height of about 70 m to allow for straightforward comparisons to the example calculation presented later. Additional parameterizations, including convection or a radiative transfer routine, are not included in the simple-physics package to ensure its reduced complexity. Radiation is excluded since it is not one of the main drivers for tropical cyclogenesis in our short ten-day simulations. In addition, both shallow and deep convection are not included as large-scale condensation appears to be a sufficient driver for the idealized tropical cyclone at high horizontal resolutions. While it is may be presumed that convection is necessary for the simulation of tropical cyclones, this is not the case. Rosenthal (1978) demonstrated that a hydrostatic model, with 20 km horizontal resolution, could simulate tropical cyclone development successfully with only large-scale condensation. Furthermore, the boundary layer scheme does not utilize sophisticated turbulence closure techniques with atmospheric stability constraints. This again ensures the simplicity of the boundary layer diffusion.

The simple-physics package is only recommended for short deterministic studies. For long-term simulations beyond e.g. 30 days, extensions such as a Newtonian temperature relaxation mechanism should be included to mimic the radiative transfer. The simple-physics package can readily be coupled to different dynamical cores to test the impact of the fluid flow package on the simulation. Another benefit of simple-physics is that each individual parameterization can be easily turned off and on, allowing for the examination of the role of each physical process. The simple-physics package thereby provides a tool for process and sensitivity studies, especially with respect to varying physics parameterizations or coefficients.

3. Description of the CAM 5 dynamical cores

The idealized tropical cyclone test case with the simple-physics suite is coupled to the four hydrostatic dynamical cores that are options in NCAR's CAM 5 model. The dynamical cores include the FV dynamical core, the SE model, and the spectral transform EUL and SLD dynamics packages (Neale et al., 2010b). These four dynamical cores are used to demonstrate the characteristics of the test case and reveal the impact of the dynamical core on the simulations. Below, we provide a brief overview of each dynamical core, and the utilized grid spacings between 156 km and 28 km, their corresponding dynamics and physics time steps, and the resolution-dependent diffusion coefficients. All CAM 5 simulations use the standard 30 vertical levels (L30) with the terrain-following hybrid σ-pressure coordinate η. The model top is placed at ≈ 2 hPa. Details about the η coordinate and its hybrid coefficients for L30 are listed in Appendix B.

3.1. Finite–Volume (FV)

The FV dynamical core is the default dynamical core in CAM versions 4 (Neale et al., 2010a), 5 and 5.1 (Neale et al., 2010b). The dynamical core is defined on a regular latitude–longitude grid that includes both pole points. The prognostic variables are staggered as in the Arakawa-D grid. The mass-conservative FV dynamical core in flux-form is built upon a 2D shallow water approach in the horizontal plane (Lin and Rood, 1996, 1997). The vertical discretization follows a "Lagrangian control-volume" principle, which is based on a terrain-following "floating" Lagrangian coordinate system and a fixed "Eulerian" reference frame. In particular, the vertically-stacked volumes are allowed to float for a duration of several dynamics time steps before they are mapped back monotonically and conservatively to a fixed hybrid reference system (Lin, 2004). The advection algorithm makes use of the monotonic third-order Piecewise Parabolic Method (PPM, Colella and Woodward (1984)) with an explicit time-stepping scheme. The algorithm also includes limiters that inherently damp grid-scale noise in the potential temperature and vorticity field. The divergent modes are controlled through explicit fourth-order horizontal divergence damping which is explained in Whitehead et al. (2011). The model is further stabilized via a Fast Fourier Transform (FFT) filter that is used in the zonal direction poleward of about 40° N/S. The dynamics and physics packages are coupled via a time-split approach.

In our study the FV dynamical core is run at the horizontal resolutions $\triangle\varphi \times \triangle\lambda$ as listed in Table 1, where $\triangle\varphi$ and $\triangle\lambda$ represent the latitudinal and longitudinal grid spacings in degrees, respectively. Table 1 also provides the approximate physical grid distances $\triangle x, \triangle y$ in the equatorial region. The time steps are represented as the subcycled dynamics time steps $\triangle\tau$ and the physics time steps $\triangle t$. The physics time step is the time interval with which the physical parameterizations are called. The FV vertical remapping algorithm is invoked every $m = 10$ subcycled dynamics time steps.

3.2. Spectral Element (SE)

The SE dynamical core is anticipated to become the default dynamical core in the future CAM release CAM 5.2. The model development and detailed design are documented in Taylor et al. (2007, 2008), Taylor and Fournier (2010), Taylor (2011) and Dennis et al. (2011). SE utilizes an explicit Runge-Kutta time stepping approach and a continuous Galerkin spectral finite element method in the horizontal directions. The latter is described in Taylor et al. (1997) and Fournier et al. (2004). The horizontal discretization is built upon unstructured quadrilaterals (a cubed-sphere mesh). In our study we select third-order polynomials that provide a fourth-order accurate horizontal discretization. These polynomials make use of 4×4 Gauss-Lobatto-Legendre (GLL) quadrature points within each spectral element.

The SE dynamical core shares some properties with the Eulerian spectral model described below. They utilize the same hybrid vertical coordinate and vertical finite-difference discretization, the horizontal diffusion scheme is based on fourth-order hyper-diffusion, and a second-order dissipation provides a sponge at the model top. The main differences are that SE uses the vector-invariant form of the momentum equations instead of the vorticity-divergence formulation as in EUL, and advects the surface pressure instead of its logarithm in order to conserve mass and energy in the dynamics package.

The physics-dynamics and tracer coupling strategy follows a hybrid paradigm. This means that the physics and dynamics packages are coupled via a process-split approach, whereas the tracer advection (e.g. for the moisture variable q) is coupled to the dynamics via time-splitting. The tracer transport scheme is built upon the same spectral element method in the horizontal, and utilizes a remapping algorithm in the vertical direction. A positive-definite constraint is applied to ensure a positive tracer mass. An offline remapping scheme called Geometrically Exact Conservative Remapping (GECoRe), explained in Ullrich et al. (2009), is used to map the model variables from the SE cubed-sphere grid to a regular latitude-longitude grid for all analyses in this study.

The horizontal resolutions, time steps and fourth-order K_4 diffusion coefficients for the SE dynamical are shown in Table 2. The resolution is defined as the number of spectral elements n_e along the edge of each cube face. These elements are further subdivided by the GLL quadrature points. A depiction of the grid and the location of the four GLL points in each element are e.g. shown in Dennis et al. (2011). The time steps in Table 2 are represented as the subcycled dynamics time steps and the physics time steps. The number of subcycles for the SE dynamical core depends on the resolution because of stability constraints. The ∇^2 horizontal diffusion coefficient K_2 in the sponge layer in the topmost three vertical levels is 2.5 $\times 10^5$ m^2 s^{-1} at all resolutions.

3.3. Eulerian Spectral Transform (EUL)

The EUL spectral transform model in vorticity-divergence form is based on the traditional three-time-level, semi-implicit spectral transform approximations applied on a quadratically unaliased Gaussian transform grid with triangular truncation (Machenhauer, 1979). The model was the default dynamical core in CAM version 3.1 and is now optional in CAM 4 and CAM 5. EUL includes the fourth-order (∇^4) hyper-diffusion in the horizontal directions applied to the vorticity and divergence equations to control the fluid flow at the smallest resolved scales. The default in the full-physics simulations (described in Section 4) also applies the ∇^4 hyper-diffusion to temperature. The K_4 diffusion coefficients are empirically chosen for each resolution to yield a reasonably straight tail for the kinetic energy spectra in model runs with parameterized physics (Boville, 1991). The model also includes a second-order ∇^2 horizontal sponge-layer diffusion at the top three levels of the model to damp upward propagating waves. The temperature equation comprises a frictional heating term that takes the heating due to the explicit momentum diffusion into account. The Eulerian dynamical core applies an *a posteriori* mass fixer at every time step. The three-time-level leapfrog method includes a time filter to control the 2 $\triangle t$ computational modes of the time stepping scheme. No global energy fixer is utilized. The physics and dynamics packages are coupled via a process-split approach.

Table 1: Horizontal grid resolutions and time steps for the FV dynamical core in CAM 5. The number of latitudes (lat) includes both pole points. The subcycled dynamics time step $\triangle\tau = \triangle t/m$ with $m = 10$ is listed, in addition to the physics time step $\triangle t$.

Resolution $\triangle\varphi \times \triangle\lambda$	No. of grid points lat $\times$ lon	Grid distance $\triangle x, \triangle y$ at equator (km)	Subcycled dynamics time step $\triangle\tau$ (s)	Physics time step $\triangle t$ (s)
$1.0^\circ \times 1.0^\circ$	181×360	111	180	1800
$0.5^\circ \times 0.5^\circ$	361×720	55	90	900
$0.25^\circ \times 0.25^\circ$	721×1440	28	45	450

Table 2: Horizontal grid resolutions, time steps and fourth-order diffusion coefficients K_4 for the SE dynamical core in CAM 5. The subcycled dynamics time steps $\triangle\tau = \triangle t/m$, the number of subcycles m and the physics time steps $\triangle t$ are listed.

Resolution n_e	No. of grid columns	Grid distance at equator (km)	Subcycled dynamics time step $\triangle\tau$ (s)	Number of subcycles m	Physics time step $\triangle t$ (s)	Diffusion coefficient K_4 (m^4 s^{-1})
30	48,602	111	360	5	1800	1.0×10^{15}
60	194,402	55	180	5	900	1.0×10^{14}
120	777,602	28	75	6	450	1.0×10^{13}

EUL utilizes a monotonic semi-Lagrangian tracer transport scheme.

Table 3 lists the horizontal resolutions, time steps and ∇^4 diffusion coefficients K_4 for the EUL dynamical core. The triangular truncation is abbreviated by T and is followed by the maximum resolvable wave number. The time step displays the dynamics time step. A subcycling mechanism for the dynamical core is optional in EUL, and is not invoked here. We call the physics package with the same $\triangle t$ frequency. However, due to the use of the leapfrog method the actual physics tendencies are applied for the duration of a $2\triangle t$ time interval since the previous $(n-1)$ time level is advanced to the future time level $(n+1)$ with the physics forcing evaluated at time level n. The base value of the ∇^2 horizontal diffusion coefficient K_2 at the third level below the model top is set to 2.5×10^5 m^2 s^{-1} for all resolutions. This K_2 coefficient is doubled at the second level below the model top, and doubled again at the topmost level.

3.4. Semi–Lagrangian Spectral Transform (SLD)

Another optional dynamical core in CAM 5 is the SLD spectral transform model. The dynamical core is based on two-time-level, semi-implicit semi-Lagrangian spectral transform approximations with quasi-cubic Lagrangian polynomial interpolants. A related three-time-level version of this dynamical core has been described in Williamson and Olson (1994). The SLD dynamical core is based on the same terrain following vertical coordinate as EUL and uses semi-Lagrangian advection in all directions. In the horizontal a triangular truncation is adopted with a quadratically unaliased Gaussian transform grid. SLD also includes the same horizontal ∇^4 hyper-diffusion and ∇^2 diffusion mechanisms as EUL. The ∇^2 horizontal diffusion again serves as a sponge in the three top model levels. As in EUL, the energy lost by the explicitly added diffusion processes acts as a frictional heating term. An *a posteriori* mass fixer is invoked at every time step. Note that the semi-Lagrangian dynamical core applies a decentering technique to damp the noise induced by orographic resonance (see Jablonowski and Williamson (2011) for a review). The default CAM 5 decentering parameter is set to $\epsilon = 0.2$. No global energy fixer is applied. The physics and dynamics packages are coupled via a process-split approach.

The SLD dynamical core utilizes the same resolutions that are used for the EUL model (see Table 3). However, the time steps $\triangle t$ are three times the corre-

Table 3: Horizontal grid resolutions, time steps and fourth-order diffusion coefficients K_4 for the EUL dynamical core in CAM 5.

Spectral resolution	No. of grid points lat $\times$ lon	Grid distance at equator (km)	Time step $\triangle t$ (s)	Diffusion coefficient K_4 (m^4 s^{-1})
T85	128×256	156	600	1.0×10^{15}
T170	256×512	78	300	1.5×10^{14}
T340	512×1024	39	150	1.5×10^{13}

sponding EUL values in Table 3. The dynamics and physics time steps are identical. The SLD dynamical core uses the same diffusion coefficients, K_4 and K_2, as the EUL package.

4. Motivation: Tropical cyclones in CAM 5 full-physics simulations

This section presents snapshots of CAM 5 full-physics simulations with each dynamical core to motivate the simulations and analysis of the simple-physics setup. A detailed description of the CAM 5 physics suite can be found in Neale et al. (2010b). The initial conditions that trigger the evolution of an idealized tropical cyclone are discussed in Appendix A. As shown below, the choice of the dynamical core has a strong impact on the 10-day simulations of the tropical storm despite the use of the identical physics package. This triggers the question whether the differences can be attributed to the characteristics of the dynamical cores, and whether the results with simpler physical forcings can replicate at least some of the differences. If yes, it might provide a pathway for an improved understanding of the highly nonlinear physics-dynamics interplay. The latter is difficult to disentangle in complex full-physics experiments. Previous high-resolution simulations with CAM 5 have shown that FV simulates intense tropical cyclones with many realistic features (Reed and Jablonowski, 2011b). Therefore, we suggest that the CAM 5 model experiments presented here and in section 5 provide a suitable basis for a dynamical core intercomparison, and challenge our understanding of both the full- and simple-physics simulations.

Figure 2 displays the wind speed at day 10 for the CAM 5 simulations using FV at 0.25°, SE at $n_e = 120$, EUL at T340 and SLD at T340. The left column of Fig. 2 shows the longitude-height cross sections of the magnitude of the wind through the center latitude of the vortex. The right column of Fig. 2 displays the horizontal cross sections of the magnitude of the wind at 100 m. The center of the vortex is defined to be the grid point with the minimum surface pressure. At day 10 the storm resembles a tropical cyclone with maximum wind speeds near the surface, a relatively calm eye and a warm-core (not shown) for each CAM 5 dynamical core. However, there is large variance amongst the dynamical cores in the cyclone intensity, the radius of maximum wind (RMW) and overall organization. In general, the FV and SE models produce a stronger storm with a smaller RMW when compared to the EUL and SLD dynamics packages. In addition, the SE package seems to produce more small-scale features when compared to FV as suggested by FV's slightly smoother contour lines. We speculate that this might be attributable to SE's higher-order (fourth-order) numerical scheme in the horizontal directions that has the potential to provide a higher nominal resolution and sharper gradients than FV. The EUL T340 dynamical core appears to simulate the weakest, least organized storm of the four dynamical cores at these high horizontal resolutions. Its RMW is the widest among the four models. There are also differences in the location of the center of the storm by day 10. This is attributed to the variance in the storm intensity and its impact on the storm's motion, which is impacted by the beta-drift effect.

The time evolution of the minimum surface pressure in the CAM 5 full-physics simulations is provided in Figure 3. Each dynamical core is run at the resolutions provided in Tables 1-3. From Figure 3 it is evident that as the horizontal resolution increases within each dynamical core the intensity of the simulated tropical cyclone increases. In all dynamical cores but EUL, there appears to be no hint of convergence of the storm intensity with increasing resolution. The EUL package might tend towards a converged simulation as the simulation at T170 and T340 approach the same minimum surface pressure at day 10. However, while the two simulations appear

to reach similar values at day 10 the path to development varies. This is evidenced by the fact that the EUL T340 simulation starts to intensify earlier in the simulation than the EUL T170 simulation. In addition, all four dynamical cores show an earlier onset of intensification with increasing resolution.

Again, Figure 3 demonstrates that at the highest resolutions, the FV and SE dynamical cores produce stronger cyclones at day 10 than the EUL and SLD dynamics packages. In general, the SE model produces the most intense tropical cyclones by day 10, and may approach unphysical minimum surface pressures at the resolution $n_e = 120$ when compared to observations. For example, the minimum surface pressure in the SE $n_e = 120$ run drops to values around 852 hPa at day 7 which are rather extreme. The lowest resolution simulations with each dynamics package all fail to completely develop over 10 simulation days, but again the FV and SE simulations develop further, as evidenced by lower surface pressures. It appears that the FV and SE dynamical cores require less horizontal resolution to simulate tropical cyclones with similar intensity to the EUL and SLD dynamical cores at higher resolutions. As an example the FV 0.5° and SE $n_e = 60$ simulations, that have grid spacings of approximately 55 km at the equator, produce similar storm intensities to the EUL T340 and SLD T340 simulations with roughly 39 km grid spacings at the equator. This is further shown in Table 4 which provides the day 10 values of the minimum surface pressure (MSP), maximum wind speed at 100 m, and center location of the tropical cyclone for all dynamical core simulations. We hypothesize that the stronger intensity of the storms could be related to the local spatial discretization techniques in the FV and SE dynamics packages, that are likely to represent locally strong gradients more reliably in contrast to the global spectral transform method in EUL and SLD.

5. Simple-physics simulations

This section presents the idealized tropical cyclone simulations of all four CAM 5 dynamical cores when coupled to the simple-physics suite. The purpose of the section is threefold. First, we assess the evolution of the tropical cyclone in FV and briefly describe the general characteristics of the simulation in section 5.1. The main aspects to consider are whether the simple-physics processes provide a suitable forcing to drive the intensification of the initial storm, and whether the tropical storm exhibits realistic features like a calm eye or slanted eye wall. Second, we provide snapshots of the dynamical core intercomparison with FV, SE, EUL and SLD in section 5.2. This reveals the impact of the dynamical core on the simplified simulations, and also assesses the convergence-with-resolution characteristics. The overarching question is whether such simple-physics experiments can help shed light on physics-dynamics interactions and whether there are similarities to full-physics runs. Third, we estimate the uncertainty of the simulations via a perturbed initial-data ensemble approach with FV (section 5.3). The latter provides insight into the robustness of the tropical cyclone simulations and the simple-physics test scenario.

Throughout the section, comparisons to the CAM 5 full-physics simulations are made. However, we do not expect to replicate the full-physics simulations, which is of course not feasible. Rather, we are interested in the general behavior of the four dynamical cores, and whether some of the sensitivities seen in full-physics simulations are present in simpler experiments. The aim is to test whether the simple-physics forcing is a suitable tool for model evaluations of intermediate complexity, and to provide an estimate of the robustness of the test case.

5.1. Evolution of the FV tropical cyclone at 0.25°

Figure 4 shows the development of the wind speed from the initial vortex for the FV 0.25° simple-physics simulation, with specific snapshots at days 3, 5 and 10. The top row (a-c) of Fig. 4 displays the horizontal cross section of the magnitude of the wind at 100 m. The bottom row (d-f) of Fig. 4 shows the longitude-height cross section of the magnitude of the wind through the center latitude of the vortex. Figure 4 offers a direct comparison to the evolution of the tropical cyclone with full CAM 5 physics as shown in Reed and Jablonowski (2011b) and Fig. 2 (top row). From Fig. 4 it is evident that the initial vortex has developed into a strong cyclone by day 3. The storm is compact and has a defined calm eye region, especially at upper levels, and has a maximum wind speed at 100 m of 73.34 m s^{-1} by day 10 (as listed later in Table 5). Figure 4 shows that the maximum wind speed occurs near the surface at the RMW, which is characteristic of tropical cyclones. In addition, the cyclone is a warm-core system (not shown).

When compared to the development of the CAM 5 full-physics storm in Reed and Jablonowski (2011b)

Table 4: Various statistics, including minimum surface pressure (MSP), maximum wind speed (MWS) at 100 m, and center location, of the tropical cyclone at day 10 for the simulations using full CAM 5 physics with each dynamical core and resolution with L30.

Model	Resolution	MSP (hPa)	MWS ($m\ s^{-1}$)	Location
FV	$1.0^\circ \times 1.0^\circ$	951.47	39.02	(169°E, 29°N)
	$0.5^\circ \times 0.5^\circ$	903.72	59.53	(170.5°E, 29.5°N)
	$0.25^\circ \times 0.25^\circ$	880.24	66.96	(167.5°E, 31.75°N)
SE	30	951.66	38.68	(170°E, 29.83°N)
	60	886.42	66.92	(167°E, 34.90°N)
	120	866.81	73.18	(162.75°E, 34.95°N)
EUL	T85	980.88	28.22	(170.16°E, 30.12°N)
	T170	918.94	53.22	(163.83°E, 29.82°N)
	T340	923.96	54.62	(163.48°E, 32.49°N)
SLD	T85	983.98	22.89	(170.16°E, 28.72°N)
	T170	943.34	41.49	(167.34°E, 29.82°N)
	T340	899.15	63.52	(165.59°E, 30.03°N)

(their Fig. 3), the simple-physics simulation is more compact, as indicated by a smaller RMW and reduced horizontal extent of the storm. This is most likely a result of the simplicity of the simple-physics package. However, the simple-physics simulation still produces an intense cyclone. The results suggest that the simple-physics suite provides suitable forcing mechanisms for the tropical cyclone, and thereby qualifies as an evaluation technique of intermediate complexity.

5.2. Dynamical core intercomparison

Figure 5, like Fig. 2, displays the wind speed at day 10, but now as simple-physics simulations using FV at 0.25°, SE at $n_e = 120$, EUL at T340 and SLD at T340. A quick comparison of the results in Fig. 5 to those in Fig. 2 shows a substantial difference between the simple-physics and CAM 5 full-physics simulations. Such differences include variations in the intensity, structure and size of the storm at day 10 for each dynamical core. In particular, all simple-physics storms are weaker than the full-physics storms, and their horizontal extent is smaller. As mentioned before these differences are expected and not the focus of the discussion here. For example, Reed and Jablonowski (2011c,b) already highlighted that structural differences of models, such as different physical parameterization suites, produce substantial variance in the evolution of the initial vortex into a tropical cyclone over ten simulation days.

Of particular interest here is whether there are similarities in the general characteristics of the storm when comparing the simple-physics and full-physics results of all dynamical cores. Figure 5 reveals such similarities. For example, the simple-physics simulations at the highest resolution with the FV and SE models produce more intense storms with smaller RMW in comparison to the cyclones in the EUL and SLD experiments. The RMW is always the widest in EUL as also shown later for other resolutions. In addition, the SE dynamical core produces the strongest storm by day 10, as seen by the maximum wind speed. When comparing the characteristics of the wind speeds in the vertical direction in Figs. 5 and 2, it is evident that the strong winds in the FV and SE models reach higher up into the atmosphere in both the simple-physics and full-physics experiments, despite the identical vertical grid and number of levels in all models.

Figure 6 presents the time evolution of the minimum surface pressure for each dynamical core and resolution with simple-physics, and can be compared to the characteristics of the full-physics runs in Fig. 3. Generally speaking, the storms in FV and SE at all "equivalent" resolutions, according to the climate analysis by Williamson (2008b) (e.g. 0.25° and T340 are equivalent), are stronger than the storms in EUL and SLD. The SE package consistently produces more intense tropical cyclones. In addition, EUL generates stronger storms

than SLD, except this similarity does not hold at the highest T340 resolution in the full-physics simulation. This general behavior could be related to the diffusion characteristics of the dynamical cores, since SLD is likely affected by enhanced numerical diffusion due to the semi-Lagrangian interpolations and its decentering mechanism. However, more in-depth analyses are necessary to test this hypothesis. As an aside, we note that the simple-physics simulations contain more temporal variations in the storm intensity in comparison to full-physics runs, as seen by the evolution of the minimum surface pressure in Fig. 6. It is likely that these variations are partially a result of the reduced nature of the precipitation processes in simple-physics since the large-scale condensation parameterization is either active or not depending on supersaturation.

Figure 6 shows that for each dynamics package as the resolution increases so does the intensity of the storm. This is furthermore evidenced by the day-10 maximum wind speed at 100 m and minimum surface pressure values provided in Table 5. When compared to Table 4, the maximum wind speeds at 100 m in Table 5 are often of the same order despite larger values for the minimum surface pressure. This can be attributed to differences in the storm's structure, mainly the location of the RMW and the lower height of the wind maximum in the simple-physics experiments. The lower height of the maximum wind speed thereby impacts the interpolated wind speeds at 100 m. In addition, Fig. 6 displays that the onset of the intensification, shown by the deepening of the minimum surface pressure, occurs sooner as the resolution increases within each dynamical core. There is no sign of convergence with resolution for any of the dynamical cores with simple-physics. The latter two aspects are also present in the full-physics simulations. Figure 6 appears to provide additional evidence that smaller grid spacings are required for the EUL and SLD models to produce comparable results to the FV and SE packages. For example, the EUL and SLD T170 simulation produce similar intensities by day 10 as the FV 1.0° and SE $n_e = 30$ simulations. Again, we speculate that this general characteristic might be related to the very different nature of the numerical discretizations. Both the FV and SE models utilize a local discretization technique in the horizontal directions which might be more favorable for the representation and intensification of such a localized storm in comparison to the global spectral method in EUL and SLD.

To complete the overall assessment Fig. 7 displays the day-10 longitude-height cross sections of the wind speed at the lower resolutions not shown in Fig. 5 for all four dynamical cores. When comparing the results in Fig. 7 with the right column of Fig. 5 is is evident that as the horizontal resolution increases the simulated storm becomes more intense and compact. Again, when comparing dynamical cores, but now the storm structure, it appears that the EUL and SLD T170 simulations are similar to the FV 1.0° and SE $n_e = 30$ simulations and the EUL and SLD T340 simulations are similar to the FV 0.5° and SE $n_e = 60$ simulations. This is consistent with the results seen earlier in Fig. 6. Note, in agreement with Fig. 6, the EUL and SLD T85 simulations fail to develop in the 10-day simulation. This is in contrast to CAM 5 full-physics simulations in which the EUL and SLD T85 storms do develop somewhat during the ten simulation days.

In summary, many general characteristics of the simple-physics simulations with all four dynamical cores are consistent with those seen in CAM 5 full-physics experiments. This encourages us to suggest that simple-physics provides a suitable physics parameterization suite to compare the impact of numerical schemes, meshes and diffusion properties on tropical storms or other flow fields.

5.3. Ensemble simulations

Our final assessment of the simple-physics suite analyzes the spread of the simulations due to small perturbations. Such ensemble runs evaluate the robustness of the unperturbed control simulation presented earlier, and provide valuable information about its uncertainty. This emphasizes that a single deterministic simulation without an uncertainty estimate has only limited significance.

This section presents the results of 11 ensemble simulations with the FV dynamical core with simple-physics. The 11 ensemble simulations consist of the control case with unperturbed initial conditions, eight simulations with random perturbations to the initial conditions and two simulations in which the longitudinal position of the center of the control vortex is shifted by $\Delta\lambda/2$ and $\Delta\lambda/4$. The eight perturbation simulations are initialized with the control vortex that is overlaid with random small-amplitude perturbations of the initial global zonal and meridional wind velocities. The random perturbations are at most ± 0.4 m s^{-1}. The simulations with the shift in the initial location of the vortex center produce small, more systematic variations in all initial

Table 5: Same with Table 4 but for the simulations using simple-physics with each dynamical core and resolution.

Model	Resolution	MSP (hPa)	MWS (m s^{-1})	Location
FV	$1.0^\circ \times 1.0^\circ$	980.04	30.77	(170°E, 25°N)
	$0.5^\circ \times 0.5^\circ$	962.45	42.87	(169°E, 24.5°N)
	$0.25^\circ \times 0.25^\circ$	937.86	73.34	(169°E, 24.5°N)
SE	30	964.95	42.97	(167°E, 33.81°N)
	60	951.22	50.11	(168.5°E, 30.41°N)
	120	921.29	76.61	(169.5°E, 27.71°N)
EUL	T85	1003.10	15.0	(168.75°E, 24.51°N)
	T170	978.28	33.40	(172.27°E, 27.02°N)
	T340	953.71	48.36	(169.80°E, 30.38°N)
SLD	T85	1002.75	14.29	(170.16°E, 27.31°N)
	T170	987.58	25.32	(168.05°E, 27.72°N)
	T340	975.24	38.22	(166.64°E, 28.27°N)

fields, since they are analytically evaluated at the grid point locations. In particular, it means that the center of the vortex now no longer coincides with a FV grid point. These shifts thereby mimic the uncertainty related to the choice of the computational grid. This choice of ensemble simulation is consistent to the initial-data uncertainty runs shown in Reed and Jablonowski (2011b) for FV simulations with the full CAM 5 physics suite. Note, that the parameter-uncertainty runs in Reed and Jablonowski (2011b) are not repeated in this paper, as the study demonstrated that there is no distinction between the initial-data and parameter uncertainty results.

Figure 8 displays the time evolution of the maximum 100 m wind speed of the simple-physics ensemble runs with FV at the horizontal resolutions (a) 1.0°, (b) 0.5° and (c) 0.25°. The control case is represented by the bold blue line, the eight runs with random perturbations to the initial wind speeds are represented by the red lines and the two runs with the shift in the initial center longitude of the vortex are represented by the green lines. It is evident from Fig. 8 that the spread in the simulations increases with increasing resolution. In fact, at the lowest 1.0° resolution there is almost no spread due the random perturbation simulations and the spread is only due to the simulations with the shift in the initial longitude of the center of the vortex. When compared to the CAM 5 FV simulations in Reed and Jablonowski (2011b) (their Fig. 8), the variations in the ensemble simulations with simple-physics are smaller at 1.0° and 0.5°. However, the variance at the horizontal resolution of 0.25° seems to be comparable for the CAM 5 full-physics and simple-physics simulations. In addition, as the resolution increases the onset of the spread occurs earlier in the evolution of the vortex. At the higher resolutions there is no distinction between the two types of initial-data uncertainty.

Figure 9 represents the spread in the simple-physics simulations as the root-mean-square deviation (RMSD) of the eight initial-data ensemble simulations from the control simulation. The evolution of the (a) minimum surface pressure and (b) the maximum 100 m wind speed for the control run are shown as the solid line and the dashed lines represent the ensemble RMSD from the control case at any given time. Again, the increase in spread with resolution is obvious in both the minimum surface pressure and the maximum wind speed. From Table 6, which shows various ensemble characteristics, it is evident that the maximum RMSD increases with resolution for both the surface pressure and wind speed. The table also shows that in most cases the absolute spread among the ensemble members increases with resolution as well. We define the absolute spread as the maximum deviation between all ensemble members at any given snapshot in time.

Figure 9 provides a sense of the robustness of the control case. At all resolutions, the control case provides a reasonable representation of the tropical cyclone. Therefore, the differences between the dynamical cores discussed in the previous section are valid even when including initial-data uncertainty. The simple-physics ex-

Table 6: Various ensemble characteristics for the minimum surface pressure and the maximum wind speed at 100 m for the simple-physics ensemble simulations at 1.0°, 0.5° and 0.25° (L30): maximum absolute spread among all ensemble members, root-mean-square deviations (RMSD) of 10 ensemble members to the control simulation at day 10, and the maximum RMSD during the 10-day simulation.

Minimum surface pressure

	Max spread	RMSD at day 10	Max RMSD
$1.0° \times 1.0°$	11.05 hPa	1.68 hPa	3.46 hPa
$0.5° \times 0.5°$	8.73 hPa	3.45 hPa	5.74 hPa
$0.25° \times 0.25°$	16.69 hPa	1.71 hPa	8.87 hPa

Maximum wind speed

	Max spread	RMSD at day 10	Max RMSD
$1.0° \times 1.0°$	7.57 m s^{-1}	0.70 m s^{-1}	2.05 m s^{-1}
$0.5° \times 0.5°$	7.98 m s^{-1}	4.74 m s^{-1}	4.74 m s^{-1}
$0.25° \times 0.25°$	12.13 m s^{-1}	4.62 m s^{-1}	5.99 m s^{-1}

periments produce a smaller ensemble spread, especially at the lower resolutions, than corresponding CAM 5 full-physics simulations. This is likely a result of the reduced complexity of the simple-physics forcing. Based on these ensemble results we again conclude that the simple-physics suite provides a suitable test scenario for dynamical core evaluations with moisture processes.

6. Summary and conclusions

This paper introduced a reduced-physics parameterization suite for AGCMs that we call "simple-physics". Simple-physics is intended to serve as a test scenario of intermediate complexity in order to build bridges between dry dynamical core assessments and moist full-physics aqua-planet and AMIP studies. Such an intermediate-complexity assessment is a missing link in the current test hierarchy, especially when evaluating the impact of the dynamical core on moist AGCM simulations.

The simplified physics suite includes parameterizations of bulk aerodynamic surface fluxes for moisture, sensible heat and momentum, vertical diffusion in the boundary layer, and large-scale condensation. It thereby contains the important driving mechanisms for tropical cyclones that serve as a specific test case. However, the simple-physics setup can also be used for other flow fields such as the analysis of mountain-induced precipitation patterns. The aims of the paper were threefold. First, we introduced all details of the simple-physics parameterization suite to ensure that it can be implemented in other models. Second, we implemented the simple-physics suite in the four dynamical cores FV, SE, EUL and SLD of NCAR's CAM 5 model, and utilized an idealized tropical cyclone test case to demonstrate the general characteristics of the simple-physics experiments. These simplified simulations were motivated by the observation that the choice of the AGCM dynamical core has a substantial impact on deterministic tropical cyclone simulations with full-physics CAM 5 in aqua-planet mode. The overarching questions were whether there are general similarities between the simple-physics and full-physics tropical cyclone simulations, and if yes whether simple-physics experiments can help shed light on the highly nonlinear physics-dynamics interplay. This might help disentangle the impact of the dynamical core in moist simulations which is difficult to evaluate in isolation in complex full-physics experiments. Third, we estimated the uncertainty of the simulations via a perturbed initial-data ensemble approach. The latter provides insight into the robustness of the tropical cyclone simulations and the simple-physics test scenario.

As expected, the simple-physics and full-physics tropical cyclone simulations show distinct differences in the structure, intensity and path of the developing storm over the 10-day simulation period. In general, the simple-physics suite produces weaker and smaller storms. These differences are due to the simplicity of the simple-physics suite and not the focus of the discussion here. Rather, the following key results were obtained

which focus on the general characteristics and similarities of the simulations with both simple-physics and full-physics.

- At the highest resolutions used in this study, FV at 0.25°, SE at $n_e = 120$, EUL at T340 and SLD at T340, all four dynamical cores produce a tropical cyclone by day 10. However, there are significant differences among them that are triggered by the dynamical core and its physics-dynamics interactions.

- The tropical cyclone in the FV at 0.25° and SE at $n_e = 120$ simulations is stronger and more compact (smaller RMW) by day 10 when compared to the EUL and SLD T340 experiments. The storm in the SE simulations is always the strongest. EUL always shows the widest RMW.

- Within each dynamical core the simulated storm becomes more intense and compact with increasing resolution. There is no sign of convergence. With increasing resolution the intensification of the tropical cyclone occurs earlier in the simulation.

- The uncertainty of the simple-physics simulations is reduced at lower resolutions in comparison to full-physics runs. At high resolutions with about 28-39 km grid spacings the uncertainty is comparable. This is likely an advantage of the simple-physics package and implies that simulations with the control vortex in the dynamical core comparisons are robust.

- The results suggest that EUL and SLD require decreased grid spacings to produce comparable results to lower-resolution experiments with FV and SE.

We suggest that the combination of simple-physics and the analytic vortex initialization technique provides a suitable basis for a test case of intermediate complexity for AGCMs. Such a test case is currently absent in the hierarchy of AGCM evaluations and developments. Using the unique framework of CAM 5 with its four dynamical cores this study has shown that the test case might be a suitable candidate for dynamical core intercomparisons.

In addition, previous studies have shown that tropical cyclones are very sensitive to physics parameterizations which makes intercomparisons of simulations with different physics packages difficult. The test case presented here allows for simplified process studies within the physics suite. For example, the sensitivity of the results to the surface flux formulation or its coefficients can easily be tested. The physics forcings can also be easily replaced by different mechanisms. This may prove to be useful for intercomparisons of AGCMs across the community, as the physics parameterization suites often vary greatly amongst different models. It may also be of particular importance with respect to the advancements in modern computer architectures that now enable AGCMs to run at higher resolutions than ever before. At these high resolutions in the km range, phenomena like tropical cyclones will likely become resolved features. As a result, it is important that the ability of such AGCMs to simulate tropical cyclones be tested during the development and evaluation stages. The test case introduced here might therefore prove to be useful in this manner.

Future work will consist of implementing the intermediate-complexity test case into other AGCM frameworks to promote model intercomparisons and in-depth analyses of the causes and effects of the modeling choices on moist simulations. In addition, the use of variable-resolution techniques, such as adaptive mesh refinement, for AGCMs is becoming a novel model design choice. The test case will be used to aid in the development of such techniques.

Acknowledgments. The authors thank Mark Taylor (Sandia National Laboratories) for his advice on the setup of SE in NCAR's CAM 5 model and Paul Ullrich (University of Michigan) for help with GECoRe. We would like to acknowledge the high performance computing support provided by NCAR's Computational and Information Systems Laboratory which is sponsored by the National Science Foundation. The work was partly supported by a Graduate Research Environmental Fellowship from the Office of Biological and Environmental Research within U.S. Department of Energy (DoE). Additional support came from the DoE's Office of Science Award No. DE-SC0003990 and Award No. DE-SC0006684.

A. Brief description of the vortex initialization

The analytic initialization technique for the model simulations is described in detail in Reed and Jablonowski (2011a). The initialization of the vortex is built upon prescribed 3D moisture, pressure, temperature and velocity fields that are embedded into tropical environmen-

tal conditions. The moisture and temperature profiles and surface pressure of the background environment fit the observed mean hurricane season sounding for the Caribbean from Jordan (1958). The background surface temperature is set to match the SST of $T_0 = 302.15$ K or 29°C and the background surface pressure is set to p_0 = 1015.1 hPa. The global background wind and therefore the wind shear is approximately zero. In addition, the topography is set to zero as required in aqua-planet experiments.

In all simulations we initialize the model with a single, initially weak, warm-core vortex in the idealized background environment. The vortex has a radius of maximum wind (RMW) of about 250 km and a 20 m s^{-1} maximum initial wind speed located at the surface. The vortex is in hydrostatic and gradient-wind balance in an axisymmetric form. Due to the analytic nature, initial conditions can be easily implemented on all CAM 5 dynamical core grids. The initial vortex has been shown to develop into a tropical cyclone-like vortex over the course of a ten-day simulation using full-physics versions of CAM 4 and CAM 5 (Reed and Jablonowski, 2011b).

B. CAM Vertical Coordinate

CAM 5 uses the orography-following hybrid σ-pressure coordinates as described in Simmons and Burridge (1981). The coordinate is a combination of a pure pressure coordination and a σ-coordinate. The pressure p at a vertical level η is given by

$$p(\lambda, \varphi, \eta, t) = a(\eta)p_{00} + b(\eta)p_s(\lambda, \varphi, t). \qquad \text{(B.1)}$$

Here λ and φ represent the longitude and latitude, respectively and t is time. The coefficients $a(\eta)$ and $b(\eta)$ are height-dependent and p_{00} is the reference pressure and is set to 10^5 Pa. For discrete representation the L full model levels are bounded by $L + 1$ interface levels. The interface levels are specified by the half indices $i + \frac{1}{2}$ and the pressure at each interface is given by

$$p_{i+\frac{1}{2}} = a_{i+\frac{1}{2}}p_{00} + b_{i+\frac{1}{2}}p_s, \qquad \text{(B.2)}$$

where $i = 0, 1, 2, ...L$. Table 7 provides the hybrid coefficients for the L =30 levels used in CAM 5 at each model level interface. The full model coefficients can be calculated from the linear average of the coefficients at the model interface below and above.

C. Partially implicit implementation of the surface fluxes

The surface fluxes are implemented with a partially implicit time stepping scheme to enhance the numerical stability. Here we use the sensible heat flux of temperature as an example. We start with the time tendency for temperature

$$\frac{\partial T_a}{\partial t} = \frac{C_H|\vec{v}_a|(T_s - T_a)}{z_a}. \qquad \text{(C.1)}$$

Next, the partial derivative of T_a with respect to t is written as a backward Euler discretization and the right-hand-side is represented in a partially implicit manner.

$$\frac{T_a^{n+1} - T_a^n}{\triangle t} = \frac{C_H|\vec{v}_a^n|(T_s - T_a^{n+1})}{z_a}. \qquad \text{(C.2)}$$

The superscripts n and $n + 1$ represent the current time step (after the update from the large-scale condensation scheme) and the future time step, respectively. Note, that on the right-hand-side of the equation the only variable taken implicitly is T_a. $|\vec{v}_a^n|$ is evaluated at the current time step and C_H is constant. The equation can now be solved for T_a^{n+1}

$$T_a^{n+1} = \frac{T_a^n + C_H|\vec{v}_a^n|T_s\frac{\triangle t}{z_a}}{1 + C_H|\vec{v}_a^n|\frac{\triangle t}{z_a}}. \qquad \text{(C.3)}$$

Similar equations for u_a, v_a and q_a can be calculated

$$u_a^{n+1} = \frac{u_a^n}{1 + C_d^n|\vec{v}_a^n|\frac{\triangle t}{z_a}} \qquad \text{(C.4)}$$

$$v_a^{n+1} = \frac{v_a^n}{1 + C_d^n|\vec{v}_a^n|\frac{\triangle t}{z_a}} \qquad \text{(C.5)}$$

$$q_a^{n+1} = \frac{q_a^n + C_E|\vec{v}_a^n|q_{sat,s}^n\frac{\triangle t}{z_a}}{1 + C_E|\vec{v}_a^n|\frac{\triangle t}{z_a}}, \qquad \text{(C.6)}$$

with the time-level dependent coefficient C_d^n. Notice that the second term in the numerator of Eq. (C.3) is absent in the case of the zonal and merdional wind. This is because the wind is set to zero at the surface.

D. Partially implicit implementation of the boundary layer diffusion

D.1. Zonal velocity

The boundary layer scheme is implemented as follows. Eq. (2.15) is written as

$$\frac{\partial u}{\partial t} = -\frac{1}{\rho}\frac{\partial F_u}{\partial z}, \qquad \text{(D.1)}$$

with $F_u = \rho\,\overline{w'u'}$. The formulations for the meridional velocity, temperature and specific humidity equations are analogous. Using the hydrostatic equation the vertical derivative is discretized as

$$-\frac{1}{\rho}\frac{\partial F_u}{\partial z} = g\frac{\partial F_u}{\partial p} = g\frac{F_{u,+} - F_{u,-}}{p_+ - p_-}, \qquad \text{(D.2)}$$

where the subscripts $+$ and $-$ denote the values at the lower and upper model interfaces, respectively. All equations and vertical discretization described in this study assume a vertical Lorenz (1960) staggering of the variables, where u, v, T and p are co-located at a full model level. In addition, we assume that p can also be evaluated at the model interfaces p_+ and p_-. Use of other vertical staggering, such as Charney and Phillips (1953) staggering, will require some reformulation of the following equations.

We now define the subscript $k = 1, 2, 3, ..., L$ that denotes the full model level, with L being the total number of full model levels. Here, the index k increases from the model top towards the surface. Then the value of $F_{u,-}$ at the upper interface of the model level k can be calculated using Eq. (2.40)

$$F_{u,-} = \rho\,\overline{w'u'} = -\rho_- K_{m,-}\frac{\partial u}{\partial z}. \qquad \text{(D.3)}$$

Using the hydrostatic approximation the equation becomes

$$F_{u,-} = g(\rho_-)^2 K_{m,-}\frac{\partial u}{\partial p}. \qquad \text{(D.4)}$$

The equation is then discretized in the partially implicit form

$$F_{u,-} = g(\rho_-^n)^2 K_{m,-}^n \frac{u_k^{n+1} - u_{k-1}^{n+1}}{p_k^n - p_{k-1}^n}. \qquad \text{(D.5)}$$

Again, the superscripts n and $n+1$ represent the current time step after the implementation of the surface-fluxes and the future time step, respectively. Note, it is assumed that the pressure does not change in time within the physics parameterizations (typical for GCMs). The upper interface density ρ_- is calculated with the help of the ideal gas law

$$\rho_-^n = \frac{2\,p_-^n}{R_d\left(T_{k-1}^n + T_k^n\right)} \qquad \text{(D.6)}$$

where the temperature at the interface is approximated via a linear average. The value for $F_{u,+}$ at the lower interface can be evaluated in a similar way

$$F_{u,+} = g(\rho_+^n)^2 K_{m,+}^n \frac{u_{k+1}^{n+1} - u_k^{n+1}}{p_{k+1}^n - p_k^n}, \qquad \text{(D.7)}$$

and density ρ_+

$$\rho_+^n = \frac{2\,p_+^n}{R_d\left(T_k^n + T_{k+1}^n\right)}. \qquad \text{(D.8)}$$

The surface fluxes $F_{u,L+}$ are set to zero.

As shown in Boville and Bretherton (2003) and Neale et al. (2010b) Eqs. (D.2), (D.5) and (D.7) represent a tridiagonal system of the form

$$-A_k^n u_{k+1}^{n+1} + B_k^n u_k^{n+1} - C_k^n u_{k-1}^{n+1} = u_k^n. \qquad \text{(D.9)}$$

Here, u_k^n represents the variable that has already been updated with the surface flux (at the lowermost model level). The super-diagonal A_k^n, diagonal B_k^n and sub-diagonal C_k^n elements (all at time level n) are

$$A_k^n = g^2(\rho_+^n)^2 K_{m,+}^n \frac{\triangle t}{(p_{k+1}^n - p_k^n)}\frac{1}{(p_+^n - p_-^n)} \qquad \text{(D.10)}$$

$$B_k^n = 1 + A_k^n + C_k^n \qquad \text{(D.11)}$$

$$C_k^n = g^2(\rho_-^n)^2 K_{m,-}^n \frac{\triangle t}{(p_k^n - p_{k-1}^n)}\frac{1}{(p_+^n - p_-^n)} \qquad \text{(D.12)}$$

We define the boundary conditions to be

$$A_L^n = 0. \qquad \text{(D.13)}$$

The boundary condition is zero because the flux from the surface has already been accounted for in the surface flux parameterization. In addition, at the model top, index $k = 1$,

$$C_1^n = 0. \qquad \text{(D.14)}$$

This ensures that there are no fluxes above the model top.

The solution to Eq. (D.9) is of the form

$$u_k^{n+1} = E_k^n u_{k-1}^{n+1} + F_k^n. \qquad \text{(D.15)}$$

We now substitute the solution (Eq. (D.15)) into Eq. (D.9)

$$u_k^{n+1} = \frac{C_k^n}{B_k^n - A_k^n E_{k+1}^n} u_{k-1}^{n+1} + \frac{u_k^n + A_k^n F_{k+1}^n}{B_k^n - A_k^n E_{k+1}^n} \qquad \text{(D.16)}$$

Therefore E_k^n and F_k^n are found to be

$$E_k^n = \frac{C_k^n}{B_k^n - A_k^n E_{k+1}} \quad \text{for } L \geq k > 1, \qquad \text{(D.17)}$$

$$F_k^n = \frac{u_k^n + A_k^n F_{k+1}^n}{B_k - A_k^n E_{k+1}^n} \quad \text{for } L \geq k > 1. \qquad \text{(D.18)}$$

From the boundary conditions

$$E^n_{L+1} = F^n_{L+1} = A^n_L = 0. \quad \text{(D.19)}$$

Again the lower boundary conditions are zero since the surface flux is computed in a seperate parameterization. The boundary condition at the top of the model Eq. (D.14) implies the following condition

$$E^n_1 = 0. \quad \text{(D.20)}$$

This boundary condition at the top of the model is the equivalent to setting the fluxes to zero above the model top. The terms E^n_k and F^n_k can be computed upwards from $k = L$. The final step is to solve Eq. (D.15) downward from the top of the model $k = 1$ to L.

D.2. Meridional velocity

The formulations above, including the boundary conditions, are analogous for the meridional velocity except Eq. (D.15) becomes

$$v^{n+1}_k = E^n_k v^{n+1}_{k-1} + F^n_k. \quad \text{(D.21)}$$

The change in formulation requires a change in the calculation of F^n_k for the meridional velocity. Therefore Eq. (D.18) becomes

$$F^n_k = \frac{v^n_k + A^n_k F^n_{k+1}}{B_k - A^n_k E^n_{k+1}} \quad \text{for } L \geq k > 1. \quad \text{(D.22)}$$

Except for these two changes the formulation of the boundary layer turbulence for the meridional velocity is identical to that of the zonal velocity explained in detail above.

D.3. Potential temperature

The implicit implementation of the boundary layer for potential temperature requires more reformulation. Mainly, the calculation of A^n_k, B^n_k and C^n_k are all altered as

$$A^n_k = g^2(\rho^n_+)^2 K^n_{E,+} \frac{\triangle t}{(p^n_{k+1} - p^n_k)} \frac{1}{(p^n_+ - p^n_-)} \quad \text{(D.23)}$$

$$B^n_k = 1 + A^n_k + C^n_k \quad \text{(D.24)}$$

$$C^n_k = g^2(\rho^n_-)^2 K^n_{E,-} \frac{\triangle t}{(p^n_k - p^n_{k-1})} \frac{1}{(p^n_+ - p^n_-)} \quad \text{(D.25)}$$

Therefore, for potential temperature E^n_k and F^n_k become

$$E^n_k = \frac{C^n_k}{B^n_k - A^n_k E_{k+1}} \quad \text{for } L \geq k > 1 \quad \text{(D.26)}$$

$$F^n_k = \frac{\Theta^n_k + A^n_k F^n_{k+1}}{B_k - A^n_k E^n_{k+1}} \quad \text{for } L \geq k > 1. \quad \text{(D.27)}$$

Again, this results in a reformulation of Eq. (D.15) for temperature

$$\Theta^{n+1}_k = E^n_k \Theta^{n+1}_{k-1} + F^n_k, \quad \text{(D.28)}$$

which leads to the temperature update

$$T^{n+1}_k = \Theta^{n+1}_k \left(\frac{p_k}{p_{00}}\right)^{R_d/c_p}. \quad \text{(D.29)}$$

Note, that the boundary conditions stated in Eq. (D.13) and Eq. (D.14) remain unchanged.

D.4. Specific humidity

The final component of the boundary layer implementation is the specific humidity q and the formulation follows closely that of the potential temperature. The calculations of A^n_k, B^n_k, C^n_k and E^n_k are the same as they are for the potential temperature (Eq. (D.23) - (D.26)). However, the formulation of F^n_k (Eq. (D.27)) becomes

$$F^n_k = \frac{q^n_k + A^n_k F^n_{k+1}}{B_k - A^n_k E^n_{k+1}} \quad \text{for } L \geq k > 1. \quad \text{(D.30)}$$

Finally, the solution of the tridiagonal system for the specific humidity is

$$q^{n+1}_k = E^n_k q^{n+1}_{k-1} + F^n_k. \quad \text{(D.31)}$$

Again the boundary conditions remain the same, as is the case for potential temperature and the zonal and meridional velocities.

References

Arakawa, A. and V. R. Lamb, 1977: Computational design of the basic dynamical process of the UCLA general circulation model. *Methods in Computational Physics*, J. Chang, Ed., Academic Press, 173–265.

Betts, A. K. and M. J. Miller, 1986: A new convective adjustment scheme, Part II: Single column tests using GATE wave, BOMEX, ATEX and arctic air-mass data sets. *Quart. J. Roy. Meteor. Soc.*, **112**, 693–709, doi: 10.1002/qj.49711247308.

Black, P. G., et al., 2007: Air sea exchange in hurricanes: Synthesis of observations from the coupled boundary layer air sea transfer experiment. *Bull. Amer. Meteor. Soc.*, **88**, 357–374, doi:10.1175/BAMS-88-3-357.

Bode, L. and R. K. Smith, 1975: A parameterization of the boundary layer of a tropical cyclone. *Bound.-Layer Meteor.*, **8**, 3–19, doi:10.1007/BF02579390.

Boer, G. J. and B. Denis, 1997: Numerical covergence of the dynamics of a GCM. *Climate Dynamics*, **13**, 359–374.

Boville, B. A., 1991: Sensitivity of simulated climate to model resolution. *J. Climate*, **4**, 469–485.

Boville, B. A. and C. S. Bretherton, 2003: Heating and kinetic energy dissipation in the NCAR Community Atmosphere Model. *J. Climate*, **16**, 3877–3887, doi:10.1175/1520-0442(2003)016<3877:HAKEDI>2.0.CO;2.

Charney, J. G. and N. A. Phillips, 1953: Numerical integration of the quasi-geostrophic equations for barotropic and simple baroclinic flows. *J. Atmos. Sci.*, **10**, 71–99, doi:10.1175/1520-0469(1953)010<0071:NIOTQG>2.0.CO;2.

Claussen, M., et al., 2002: Earth system models of intermediate complexity: closing the gap in the spectrum of climate system models. *Climate Dynamics*, **18 (7)**, 579–586.

Colella, P. and P. R. Woodward, 1984: The Piecewise Parabolic Method (PPM) for gas-dynamical simulations. *J. Comput. Phys.*, **54**, 174–201, doi:10.1016/0021-9991(84)90143-8.

Dennis, J., et al., 2011: CAM-SE: A scalable spectral element dynamical core for the Community Atmosphere Model. *Int. J. High Performance Computing Applications*, doi:10.1177/1094342011428142, published online on 11/14/2011.

Fournier, A., M. A. Taylor, and J. J. Tribbia, 2004: The spectral element atmospheric model: High-resolution parallel computation and response to regional forcing. *Mon. Wea. Rev.*, **132**, 726–748.

Frierson, D. M. W., I. M. Held, and P. Zurita-Gotor, 2006: A gray-radiation aquaplanet moist GCM. Part I: Static stability and Eddy scale. *J. Atmos. Sci.*, **63**, 2548–2566, doi:10.1175/JAS3753.1.

Galewsky, J., L. M. Polvani, and R. K. Scott, 2004: An initial-value problem to test numerical models of the shallow water equations. *Tellus*, **56A**, 429–440.

Garratt, J. R., 1992: *The Atmospheric Boundary Layer*. Cambridge University Press, 316 pp.

Gates, W. L., 1992: AMIP: The Atmospheric Model Intercomparison Project. *Bull. Amer. Meteor. Soc.*, **73**, 1962–1970.

Gates, W. L., et al., 1999: An overview of the results of the Atmospheric Model Intercomparison Project (AMIP I). *Bull. Amer. Meteor. Soc.*, **80**, 29–55.

Giraldo, F. X. and T. E. Rosmond, 2004: A scalable Spectral Element Eulerian Atmospheric Model (SEE-AM) for NWP: Dynamical core tests. *Mon. Wea. Rev.*, **132**, 133–153, doi:10.1175/1520-0493(2004)132<0133:ASSEEA>2.0.CO;2.

Hasse, L. and S. D. Smith, 1997: Local sea surface wind, wind stress, and sensible and latent heat fluxes. *J. Climate*, **10**, 2711–2724, doi:10.1175/1520-0442(1997)010.

Held, I. M. and M. J. Suarez, 1994: A proposal for the intercomparison of the dynamical cores of atmospheric general circulation models. *Bull. Amer. Meteor. Soc.*, **75**, 1825–1830, doi:10.1175/1520-0477(1994)075<1825:APFTIO>2.0.CO;2.

Holton, J. R., 2004: *An Introduction to Dynamic Meteorology*. 4th ed., Elsevier Acadamic Press, ISBN 0123540151, 535 pp.

Jablonowski, C., P. H. Lauritzen, R. D. Nair, and M. A. Taylor, 2008: Idealized test cases for the dynamical cores of Atmospheric General Circulation Models: A proposal for the NCAR ASP 2008 summer colloquium, available online at http://www-personal.umich.edu/~cjablono/cv.html#Publication.

Jablonowski, C. and D. L. Williamson, 2006: A baroclinic instabilitiy test case for atmospheric model dynamical cores. *Quart. J. Roy. Meteor. Soc.*, **132 (621C)**, 2943–2975.

Jablonowski, C. and D. L. Williamson, 2011: The pros and cons of diffusion, filters and fixers in atmospheric general circulation models. *Numerical Techniques for Global Atmospheric Models*, P. H. Lauritzen, C. Jablonowski, M. A. Taylor, and R. D. Nair,

Eds., Springer, Lecture Notes in Computational Science and Engineering, Vol. 80, 381–493.

Jordan, C. L., 1958: Mean soundings for the west indies area. *J. Atmos. Sci.*, **15**, 91–97, doi:10.1175/1520-0469(1958)015.

Lauritzen, P. H., C. Jablonowski, M. A. Taylor, and R. D. Nair, 2010: Rotated versions of the Jablonowski steady-state and baroclinic wave test cases: A dynamical core intercomparison. *J. Adv. Model. Earth Syst.*, **2**, 34 pp., doi:10.3894/JAMES.2010.2.15, #15.

Lin, S.-J., 2004: A "vertically Lagrangian" finite-volume dynamical core for global models. *Mon. Wea. Rev.*, **132**, 2293–2307.

Lin, S.-J. and R. B. Rood, 1996: Multidimensional flux-form semi-Lagrangian transport scheme. *Mon. Wea. Rev.*, **124**, 2046–2070.

Lin, S.-J. and R. B. Rood, 1997: An explicit flux-form semi-Lagrangian shallow water model on the sphere. *Quart. J. Roy. Meteor. Soc.*, **123**, 2477–2498.

Lorenz, E. N., 1960: Energy and numerical weather prediction. *Tellus*, **12**, 364–373.

Machenhauer, B., 1979: The spectral method. *Numerical methods used in atmospheric models*, A. Kasahara, Ed., GARP Publications Series No 17, WMO and ICSU, Geneva, Vol. 2, 121–275.

Mishra, S. K., M. A. Taylor, R. D. Nair, P. H. Lauritzen, H. M. Tufo, and J. J. Tribbia, 2011: Evaluation of the HOMME dynamical core in the aquaplanet configuration of NCAR CAM4: Rainfall. *J. Climate*, **24**, 4037–4055.

Molteni, F., 2002: Atmospheric simulations using a GCM with simplified physical parametrizations. I: model climatology and variability in multi-decadal experiments. *Climate Dynamics*, **20**, 175–191, doi:10.1007/s00382-002-0268-2.

Monaco, A. V. and R. T. Williams, 1975: An atmospheric global prediction model using a modified Arakawa differencing scheme. Tech. rep., Dept. of Meteorology, Naval Postgraduate School, Monterey, CA. NPS-51WU75041, 86pp.

Neale, R. B. and B. J. Hoskins, 2000: A standard test for AGCMs including their physical parametrizations: I: the proposal. *Atmos. Sci. Letters*, **1**, 101–107, doi:10.1006/asle.2000.0019.

Neale, R. B., et al., 2010a: Description of the NCAR Community Atmosphere Model (CAM 4.0). NCAR Technical Note NCAR/TN-485+STR, National Center for Atmospheric Research, Boulder, Colorado. 212 pp., available from http://www.cesm.ucar.edu/models/cesm1.0/cam/.

Neale, R. B., et al., 2010b: Description of the NCAR Community Atmosphere Model (CAM 5.0). NCAR Technical Note NCAR/TN-486+STR, National Center for Atmospheric Research, Boulder, Colorado. 268 pp., available from http://www.cesm.ucar.edu/models/cesm1.0/cam/.

Polvani, L. M., R. K. Scott, and S. J. Thomas, 2004: Numerically Converged Solutions of the Global Primitive Equations for Testing the Dynamical Core of Atmospheric GCMs. *Mon. Wea. Rev.*, **132**, 2539–2552, doi:10.1175/MWR2788.1.

Randall, D. A., K.-M. Xu, R. J. C. Somerville, and S. Iacobellis, 1996: Single-column models and cloud ensemble models as links between observations and climate models. *J. Climate*, **9**, 1683–1697, doi:10.1175/1520-0442(1996)009¡1683:SCMACE¿2.0.CO;2.

Reed, K. A. and C. Jablonowski, 2011a: An analytic vortex initialization technique for idealized tropical cyclone studies in AGCMs. *Mon. Wea. Rev.*, **139**, 689–710, doi:10.1175/2010MWR3488.1.

Reed, K. A. and C. Jablonowski, 2011b: Assessing the uncertainty of tropical cyclone simulations in NCAR's Community Atmosphere Model. *J. Adv. Model. Earth Syst.*, **3**, M08 002, doi:10.1029/2011MS000076, 16 pp.

Reed, K. A. and C. Jablonowski, 2011c: Impact of physical parameterizations on idealized tropical cyclones in the Community Atmosphere Model. *Geophys. Res. Lett.*, **38**, L04 805, doi:10.1029/2010GL046297.

Rosenthal, S. L., 1978: Numerical Simulation of Tropical Cyclone Development with Latent Heat Release by the Resolvable Scales I: Model Description and Preliminary Results. *Journal of Atmospheric Sciences*, **35**, 258–271, doi:10.1175/1520-0469(1978)035<0258:NSOTCD>2.0.CO;2.

Simmons, A. J. and D. M. Burridge, 1981: An energy and angular-momentum conserving vertical finite-difference scheme and hybrid vertical coordinates. *Mon. Wea. Rev.*, **109**, 758–766.

Smith, R. K. and S. Vogl, 2008: A simple model of the hurricane boundary layer revisited. *Quart. J. Roy. Meteor. Soc.*, **134**, 337–351, doi:10.1002/qj.216.

Taylor, M., J. Tribbia, and M. Iskandarani, 1997: The spectral element method for the shallow water equations on the sphere. *J. Comput. Phys.*, **130**, 92–108.

Taylor, M. A., 2011: Conservation of mass and energy for the moist atmospheric primitive equations on unstructured grids. *Numerical Techniques for Global Atmospheric Models*, P. H. Lauritzen, C. Jablonowski, M. A. Taylor, and R. D. Nair, Eds., Springer, Lecture Notes in Computational Science and Engineering, Vol. 80, 357–380.

Taylor, M. A., J. Edwards, and A. St-Cyr, 2008: Petascale atmospheric models for the Community Climate System Model: New developments and evaluation of scalable dynamical cores. *Journal of Physics: Conference Series*, **125**, 012 023.

Taylor, M. A., J. Edwards, S. Thomas, and R. D. Nair, 2007: A mass and energy conserving spectral element atmospheric dynamical core on the cubed-sphere grid. *Journal of Physics: Conference Series*, **78**, 012 074, available online at http://www.iop.org/EJ/toc/1742-6596/78/1.

Taylor, M. A. and A. Fournier, 2010: A compatible and conservative spectral element method on unstructured grids. *J. Comput. Phys.*, **229**, 5879–5895.

Tiedtke, M., 1987: Parametrization of non-convective condensation processes. Lecture Notes NWP Course Parametrization of Diabatic Processes, European Centre for Medium-Range Weather Forecasts, Reading, U.K. 11 pp.

Ullrich, P. A., P. H. Lauritzen, and C. Jablonowski, 2009: Geometrically Exact Conservative Remapping (GECoRe): Regular Latitude-Longitude and Cubed-Sphere Grids. *Mon. Wea. Rev.*, **137**, 1721–1741, doi:10.1175/2008MWR2817.1.

White, A. A., B. J. Hoskins, I. Roulstone, and A. Staniforth, 2005: Consistent approximate models of the global atmosphere: shallow, deep, hydrostatic, quasi-hydrostatic and non-hydrostatic. *Quart. J. Roy. Meteor. Soc.*, **131**, 2081–2107.

Whitehead, J., C. Jablonowski, R. B. Rood, and P. H. Lauritzen, 2011: A stability analysis of divergence damping on a latitude-longitude grid. *Mon. Wea. Rev.*, **139**, 2976–2993.

Williamson, D. L., 2002: Time-split versus process-split coupling of parameterizations and dynamical core. *Mon. Wea. Rev.*, **130**, 2024–2041, doi:10.1175/1520-0493(2002)130<2024:TSVPSC>2.0.CO;2.

Williamson, D. L., 2008a: Convergence of aqua-planet simulations with increasing resolution in the Community Atmospheric Model, Version 3. *Tellus*, **60**, 848–862, doi:10.1111/j.1600-0870.2008.00339.x.

Williamson, D. L., 2008b: Equivalent finite volume and Eulerian spectral transform horizontal resolutions established from aqua-planet simulations. *Tellus*, **60**, 839–847, doi:10.1111/j.1600-0870.2008.00340.x.

Williamson, D. L., J. B. Drake, J. J. Hack, R. Jakob, and P. N. Swarztrauber, 1992: A standard test set for numerical approximations to the shallow water equations in spherical geometry. *J. Comput. Phys.*, **102**, 211–224, doi:10.1016/S0021-9991(05)80016-6.

Williamson, D. L. and J. G. Olson, 1994: Climate simulations with a semi-Lagrangian version of the NCAR Community Climate Model. *Mon. Wea. Rev.*, **122 (7)**, 1594–1610.

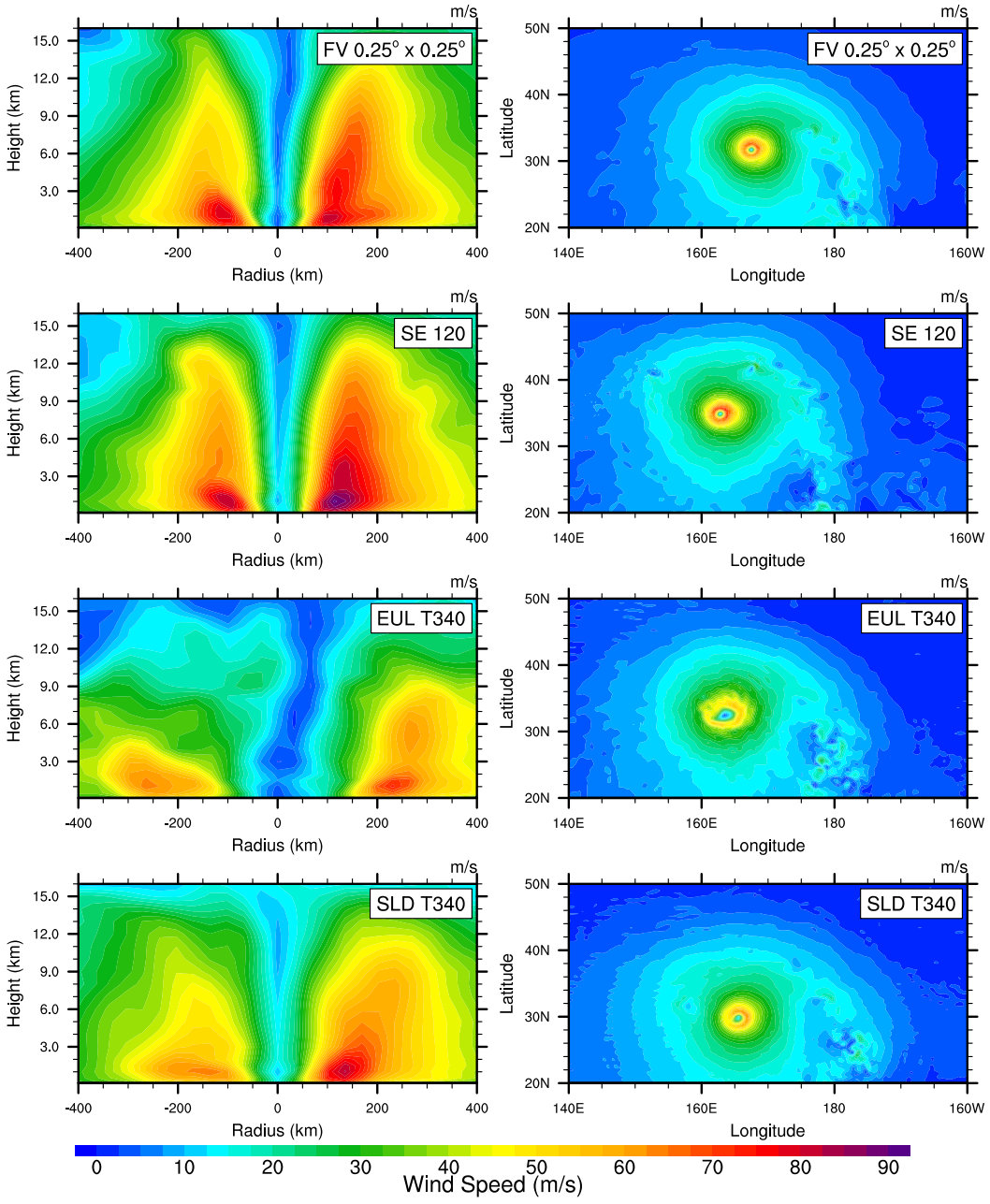

Figure 2: Snapshot of the tropical cyclone at day 10 for each dynamical core (FV, SE, EUL and SLD) with full CAM 5 physics at the highest respective resolution and L30 used for this study (as labeled). Left column: longitude-height cross section of the wind speed through the center latitude of the vortex as a function of the radius from the vortex center. Right column: horizontal cross section of the wind speed at a height of 100 m.

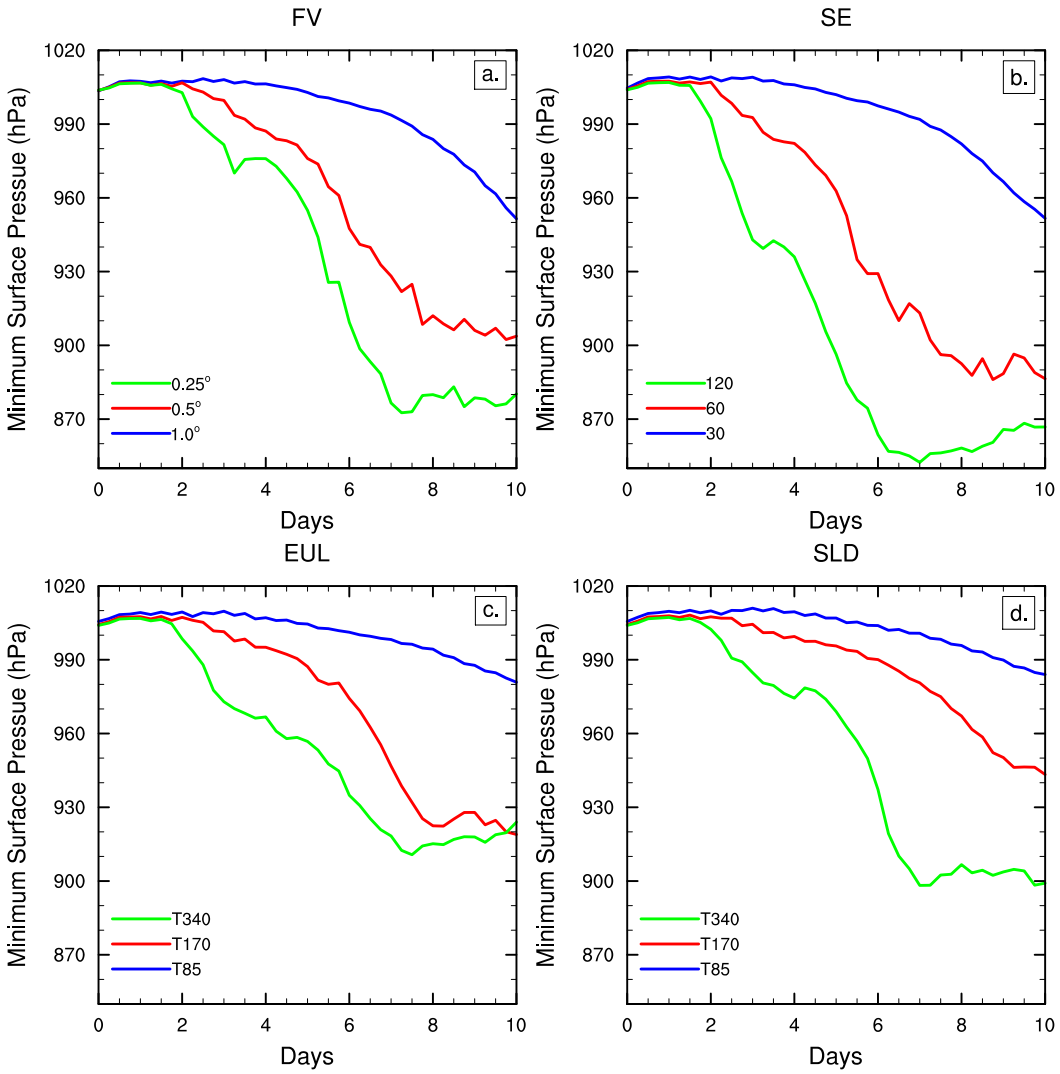

Figure 3: Time evolution of the minimum surface pressure of the tropical cyclone with full CAM 5 physics and the (a) FV, (b) SE, (c) EUL and (d) SLD dynamical cores. These L30 simulations use the horizontal resolutions provided in Tables 1-3.

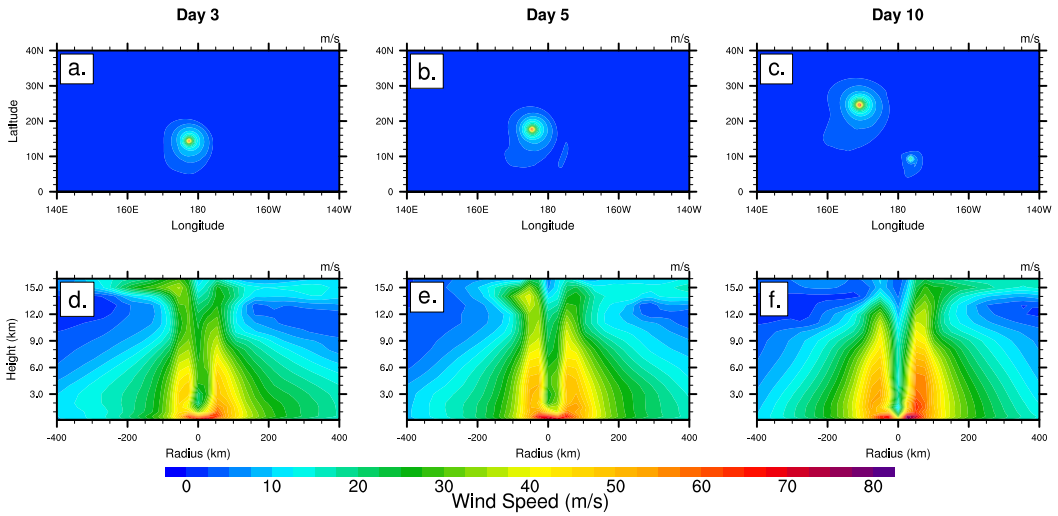

Figure 4: Snapshots of the tropical cyclone at day 3 (left), 5 (middle) and day 10 (right) with CAM 5 FV at the resolution 0.25° L30 for simple-physics. Top row (a-c): horizontal cross section of the wind speed at a height of 100 m. Bottom row (d-f): longitude-height cross section of the wind speed through the center latitude of the vortex as a function of the radius from the vortex center.

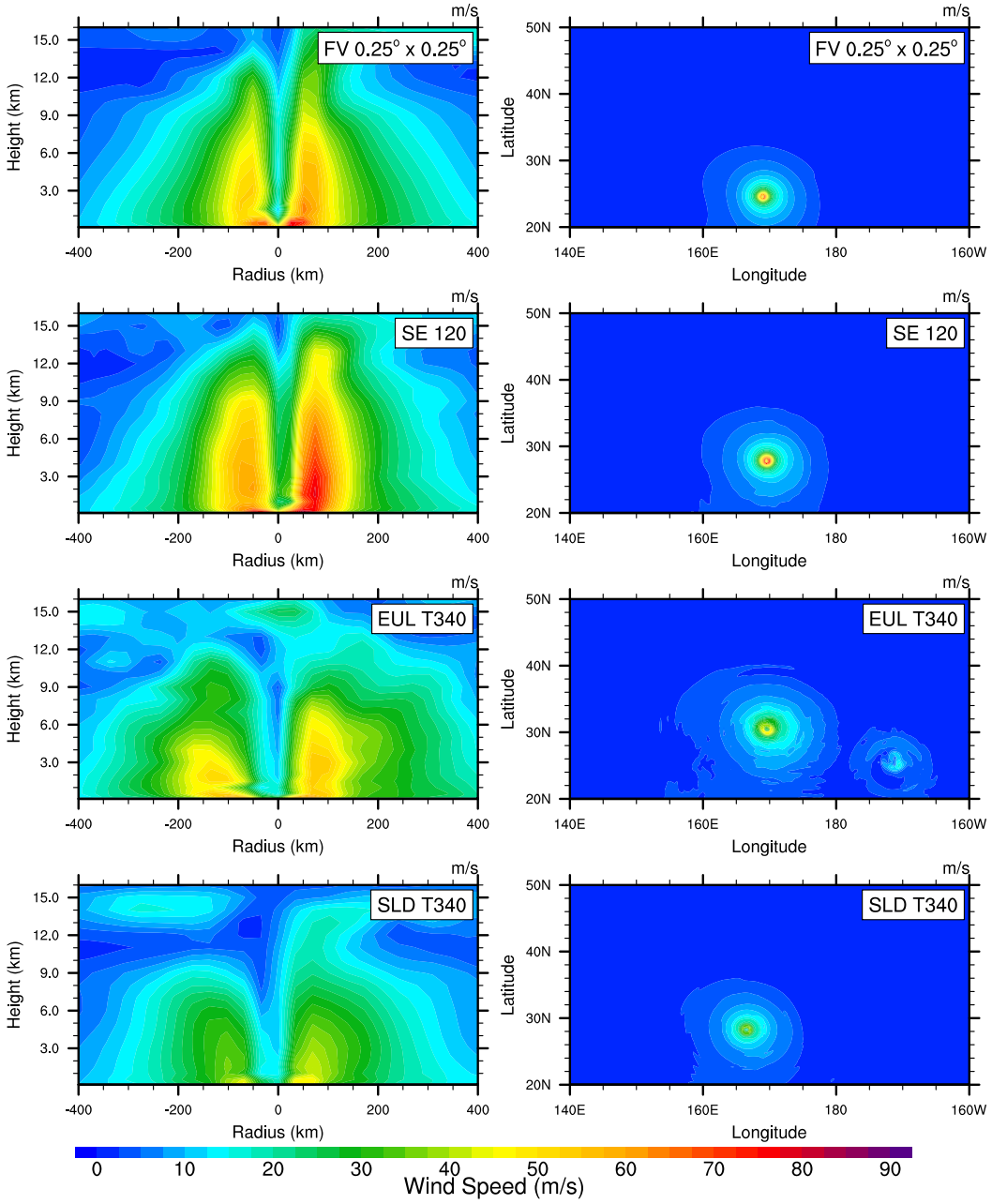

Figure 5: Same as Fig. 2 but for the simple-physics simulations.

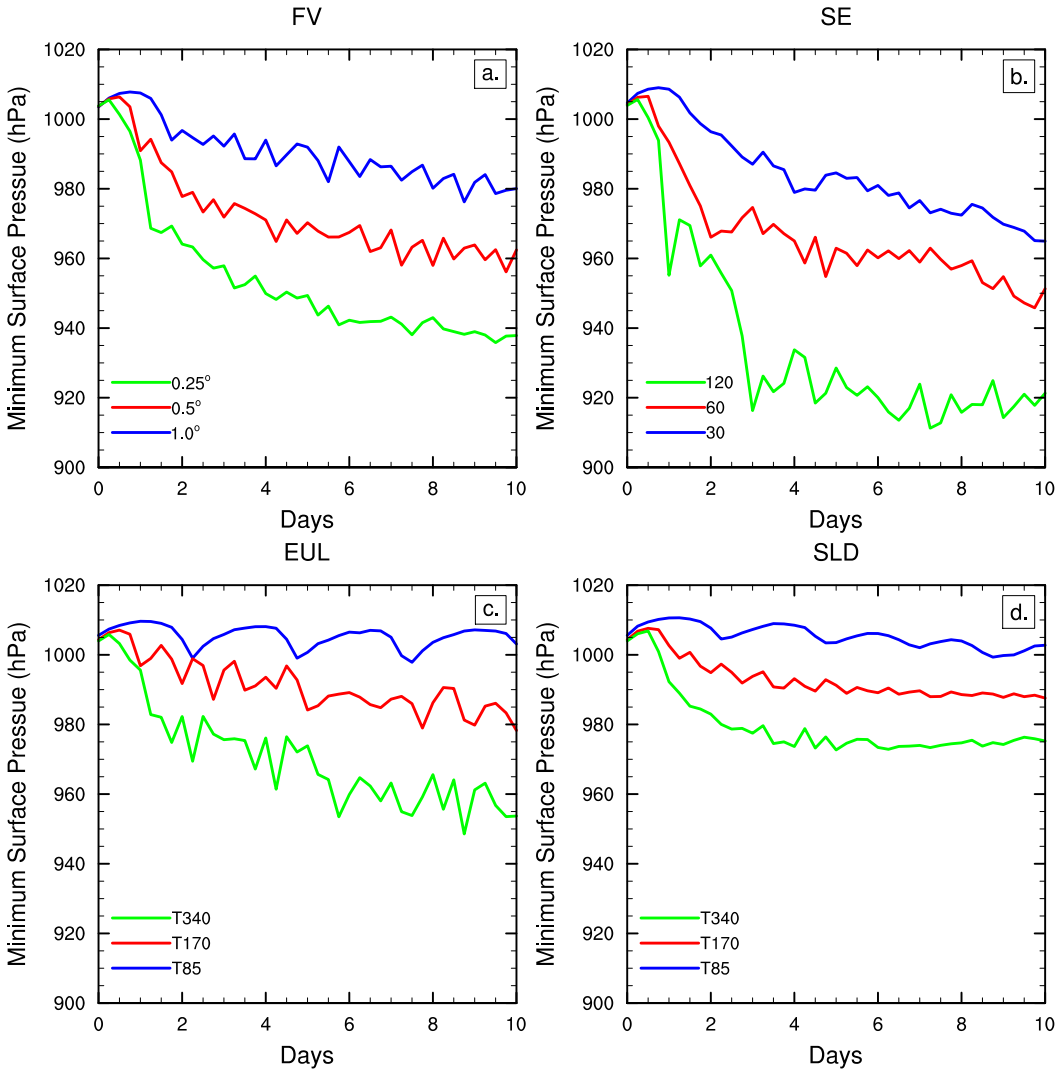

Figure 6: Same as Fig. 3 but for the simple-physics simulations.

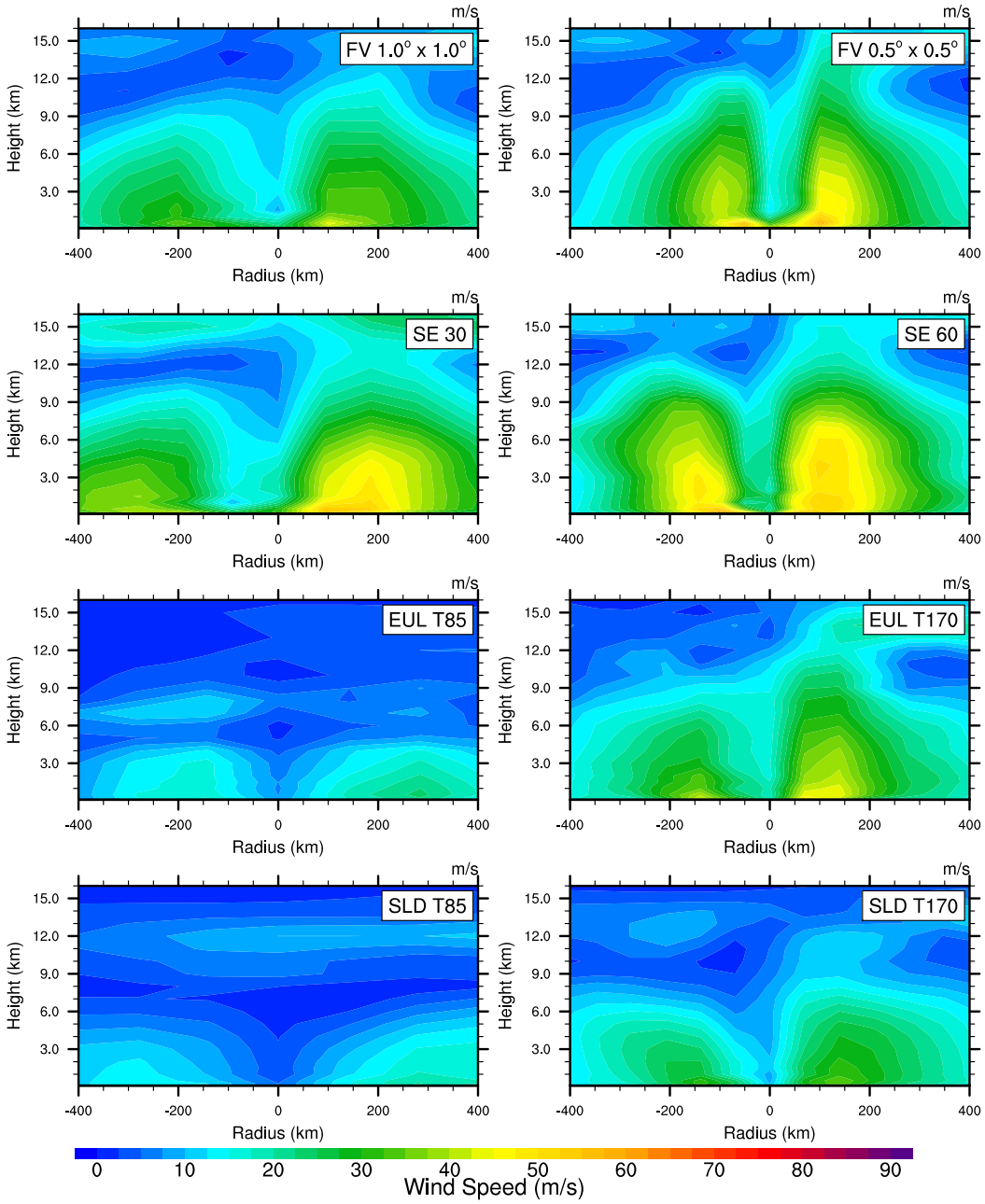

Figure 7: Snapshot of the tropical cyclone at day 10 for FV, SE, EUL and SLD with simple-physics at the remaining horizontal resolutions (as labeled, with L30) not shown in Fig. 5. The results are displayed as a longitude-height cross section of the wind speed through the center latitude of the vortex as a function of the radius from the vortex center.

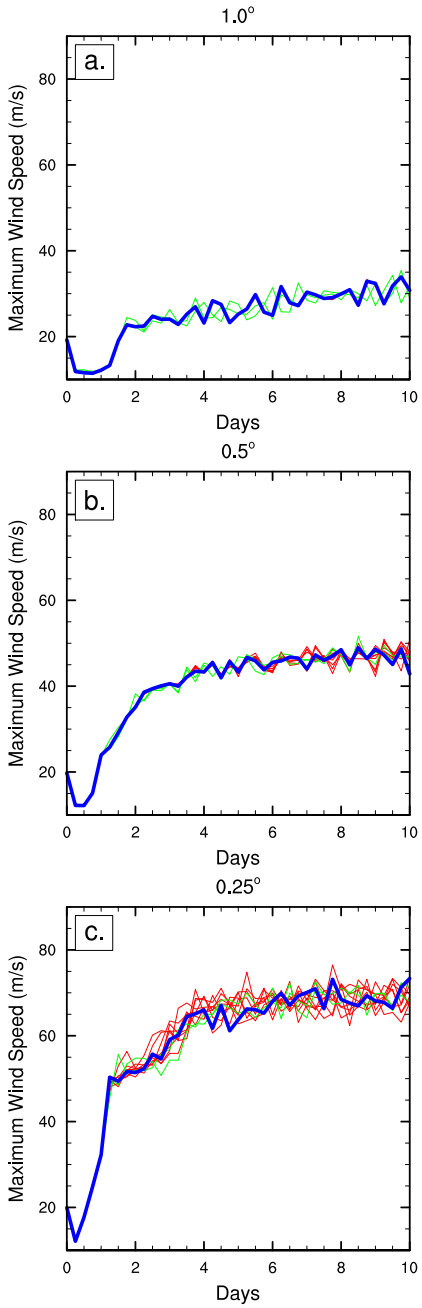

Figure 8: Time evolution of the maximum wind speed at 100 m of the ensemble simulations with simple-physics at FV (a) 1.0°, (b) 0.5° and (c) 0.25° with L30. The bold blue line represents the unperturbed control case, the red lines represent the eight runs with random perturbations to the initial zonal and meridional wind speeds and the green lines represent the two runs with the shift in the initial center longitude of the vortex.

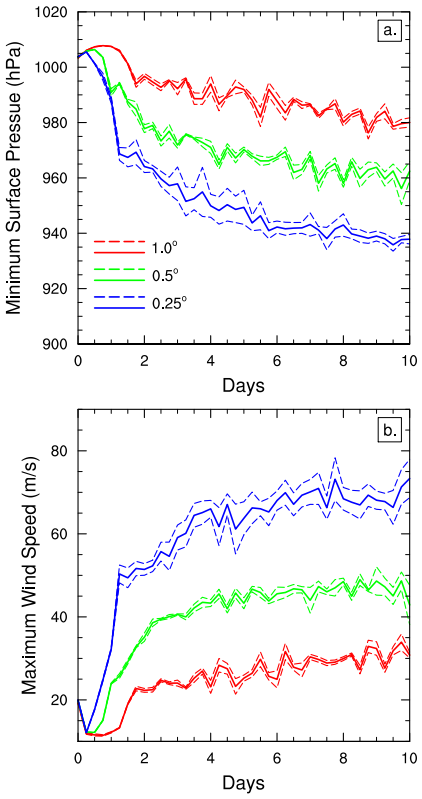

Figure 9: Time evolution of the minimum surface pressure (top) and maximum wind speed at 100 m (bottom) of the control case at the horizontal resolutions of the FV 1.0° (red), 0.5° (green) and 0.25° (blue) with simple-physics (L30). The solid line represents the unperturbed control case, the dashed lines represent the variance as determined by the ensemble RMSD.

Table 7: Vertical hybrid coefficients at level interfaces for the CAM 5 30-level setup. The coefficient $a_{i+\frac{1}{2}}$ represents the pure pressure component and $b_{i+\frac{1}{2}}$ denotes the σ-pressure component, with the subscript $i+\frac{1}{2}$ defining the model interface between two full model levels.

i	$a_{i+\frac{1}{2}}$	$b_{i+\frac{1}{2}}$
0	0.00225523952394724	0.
1	0.00503169186413288	0.
2	0.0101579474285245	0.
3	0.0185553170740604	0.
4	0.0306691229343414	0.
5	0.0458674766123295	0.
6	0.0633234828710556	0.
7	0.0807014182209969	0.
8	0.0949410423636436	0.
9	0.11169321089983	0.
10	0.131401270627975	0.
11	0.154586806893349	0.
12	0.181863352656364	0.
13	0.17459799349308	0.0393548272550106
14	0.166050657629967	0.0856537595391273
15	0.155995160341263	0.140122056007385
16	0.14416541159153	0.204201176762581
17	0.130248308181763	0.279586911201477
18	0.113875567913055	0.368274360895157
19	0.0946138575673103	0.47261056303978
20	0.0753444507718086	0.576988518238068
21	0.0576589405536652	0.672786951065063
22	0.0427346378564835	0.753628432750702
23	0.0316426791250706	0.813710987567902
24	0.0252212174236774	0.848494648933411
25	0.0191967375576496	0.881127893924713
26	0.0136180268600583	0.911346435546875
27	0.00853108894079924	0.938901245594025
28	0.00397881818935275	0.963559806346893
29	0.	0.985112190246582
30	0.	1.